THESIS FOR THE DEGREE OF DOCTOR OF PHILOSOPHY

Oxygen Carriers Materials for Chemical-Looping Technologies

-Reactivity and Kinetics

Muhammad Qamar ul Islam Zafar

Department of Chemical and Biological Engineering
CHALMERS UNIVERSITY OF TECHNOLOGY
Göteborg, Sweden 2007

Oxygen Carriers Materials for Chemical-Looping Technologies
-Reactivity and Kinetics
Muhammad Qamar ul Islam Zafar

ISBN 978-91-7291-929-7

Doktorsavhandlingar vid Chalmers tekniska högskola
Ny serie Nr 2610
ISSN 346-718X

Department of Chemical and Biological Engineering
CHALMERS UNIVERSITY OF TECHNOLOGY
SE- 412 96 Göteborg
Sweden
Telephone: +46 (031) - 772 10 00

Chalmers Reproservice
Göteborg, Sweden 2007

Abstract

Carbon dioxide is the gas which contributes most to the greenhouse effect. It is released in large quantities from fossil fuel-based power plants around the world. It is generally accepted that a rapid decrease in the emissions of carbon dioxide is needed. One method to achieve rapid reductions in the emissions and still use fossil fuels is to capture and store the carbon dioxide. However, the separation of carbon dioxide from a flue gas stream of a power plant is an expensive and energy-intensive process resulting in a large decrease in efficiency. Thus there is a need to find cheaper and more efficient methods to perform the separation. Chemical-looping combustion (CLC) and chemical-looping reforming (CLR) are innovative technologies for power and hydrogen production from natural gas with the capture of carbon dioxide. In CLC, CO_2 is inherently separated from other flue gas components i.e. N_2 and O_2 with minor energy losses. With some modifications CLC can be modified for production of hydrogen, i.e. CLR. Both processes involve the use of an oxygen carrier that transfers oxygen from combustion air to the fuel. Two inter-connected fluidized beds, a fuel and an air reactor, are used in the process. Whereas the natural gas is fully oxidized to CO_2 and H_2O in the fuel reactor for CLC, it is only partially oxidized by the metal oxide in the fuel reactor for CLR, resulting in a mixture of H_2, CO_2, CO and H_2O. The exit stream from the fuel reactor can be sent to a water gas shift reactor to get an undiluted stream of CO_2 and H_2. The reduced metal oxide is sent into the air reactor where it is oxidized by air. The oxidation reaction is exothermic resulting in heat production in the air reactor. This heat is used to maintain the oxygen carrier particles at the high temperature necessary for the endothermic reaction in the fuel reactor. The hot gases exiting from the air reactor can be used for power production.

For the chemical-looping technologies to become successful it is important to find suitable oxygen carriers. This thesis focuses on the development and reactivity testing of such oxygen carriers. For CLR, metal oxides based on Ni, Cu, Mn and Fe were prepared by impregnation on SiO_2 and $MgAl_2O_4$ and tested in a laboratory fluidized bed reactor as well as a thermogravimetric analyzer (TGA). The particles were exposed to alternating reducing (50% CH_4/ 50% H_2O) and oxidizing (5% O_2) conditions. With respect to the metal oxides on the SiO_2 support, the particles based on NiO and CuO showed the highest reactivity, whereas Fe_2O_3 and Mn_2O_3 showed signs of deactivation as function of cycle number, likely due to the formation of metallic silicates. Only NiO showed high selectivity toward H_2. All the $MgAl_2O_4$-supported metal oxides exhibited high reactivity under reducing and oxidizing conditions. In contrast to the SiO_2 based particles, no deactivation as a function of cycle number was seen for any of these oxygen carriers.

Reduction and oxidation kinetics of oxygen carriers of $NiO/MgAl_2O_4$ and $Mn_3O_4/Mg\text{-}ZrO_2$ for CLC were investigated using methane and air in a TGA. At high temperature both oxygen carriers reacted rapidly under both reducing and oxidizing conditions and the reaction rate was a function of the temperature and concentration of reacting gas. However, it was found that $NiO/MgAl_2O_4$ may not be feasible to be used below 900 °C due to low reactivity. The reactions were modeled using the shrinking-core model for spherical grains assuming chemical reaction control and the kinetic parameters were calculated for both oxygen carriers. From the kinetic parameters the solid inventories in a real CLC system were calculated. The minimum solid inventories needed were 22 kg/MW_f for $NiO/MgAl_2O_4$ and 135 kg/MW_f for $Mn_3O_4/Mg\text{-}ZrO_2$. These masses are very low compared to other oxygen carriers investigated previously, and thus both type of particles are very promising for a real CLC system.

Keywords: Chemical-looping combustion, Chemical-looping reforming, Natural gas, CO_2, Oxygen carriers, Reaction kinetics, TGA, Metal oxides

List of papers

This thesis is based on the following papers:

I. **Integrated Hydrogen and Power Production with CO_2 Capture Using Chemical-Looping Reforming-Redox Reactivity of Particles of CuO, Mn_2O_3, NiO, and Fe_2O_3 Using SiO_2 as a Support**
Qamar Zafar, Tobias Mattisson, Börje Gevert
Ind. Eng. Chem. Res., **2005**, *44, 3485-3496*

II. **Redox investigation of Some Oxides of Transition State Metals Ni, Cu, Fe and Mn Supported on SiO_2 and $MgAl_2O_4$**
Qamar Zafar, Tobias Mattisson, Börje Gevert
Energy & Fuels, **2006**, *20, 34-44*

III. **Reaction Kinetics of Freeze-Granulated $NiO/MgAl_2O_4$ Oxygen Carrier Particles for Chemical-Looping Combustion**
Qamar Zafar, Alberto Abad, Tobias Mattisson, Börje Gevert
Energy & Fuels, **2007**, *21, 610-618*

IV. **Reduction and Oxidation Kinetics of Mn_3O_4/Mg-ZrO_2 Oxygen Carrier Particles for Chemical-Looping Combustion**
Qamar Zafar, Alberto Abad, Tobias Mattisson, Börje Gevert, Michael Strand
Submitted for Publication, **2007**

Contribution by Qamar Zafar to papers I - IV

I. Responsible for all experimental work, evaluation of experimental data and writing.
II. Responsible for all experimental work, evaluation of experimental data and writing.
III. Responsible for all experimental work, evaluation of experimental data and writing.*
IV. Responsible for all experimental work, evaluation of experimental data and writing.*

* The reaction models were developed by Alberto Abad.

List of related papers not included in the thesis

V. Chemical-Looping Combustion a New CO_2 Management Technology

Tobias Mattisson, Qamar Zafar, Marcus Johansson, Anders Lyngfelt

1st Regional Symposium on Carbon Management, Dhahran, Saudi Arabia 21-24 May **2006**.

VI. Integrated Hydrogen and Power Production from Natural Gas with CO_2 Capture

Tobias Mattisson, Qamar Zafar, Anders Lyngfelt, Börje Gevert

15th World Hydrogen Energy Conference, Yokohama, Japan 27 June-2 July **2004**.

CONTENTS

1. Introduction 1

2. Objective 2

3. Background 2

4. Chemical-looping technologies 4

4.1 Chemical-looping combustion 4

4.1.1 CLC reactor design 5

4.2 Chemical-looping reforming 6

4.3 Oxygen carriers 7

5. Experimental work 10

5.1 Preparation of oxygen carriers 10

5.1.1 Impregnation 10
5.1.2 Freeze granulation 10

5.2 Characterization of oxygen carriers 11

5.3 Experimental methods 11

5.4 Experiments in laboratory fluidized bed reactor 12

5.5 Experiments in thermogravimetric analyzer (TGA) 14

5.6 Data evaluation 16

6. Gas-solid reaction models 18

7. Results 22

7.1 Investigation of SiO_2 supported oxygen carriers in fluidized bed 22

7.1.1 Reactivity during reduction and oxidation 23
7.1.2 Effect of temperature 24
7.1.3 Effect of cycle number 25
7.1.4 Carbon deposition 25
7.1.5 Selectivity towards H_2 formation 26

7.2 Investigation of $MgAl_2O_4$ and SiO_2 supported oxygen carriers in TGA 26

7.2.1 Conversion 26
7.2.2 Reduction rate 28
7.2.3 Oxidation rate 28
7.2.4 Effect of cycle number 29
7.2.5 Effect of temperature 29

7.3 Reduction and oxidation kinetics for $NiO/MgAl_2O_4$ oxygen carrier 30

7.3.1 Reduction reaction 31
7.3.2 Oxidation reaction 33
7.3.3 Amount of $NiO/MgAl_2O_4$ in the fuel and air reactor 34

7.4 Reduction and oxidation kinetics for the Mn_3O_4/Mg-ZrO_2 oxygen carrier 35

7.4.1 Reduction reaction 35
7.4.2 Oxidation reaction 38
7.4.3 Recirculation rate and solid inventory for the Mn_3O_4/Mg-ZrO_2 oxygen carrier 39

8. Discussion 42

9. Conclusions.....46

10. Notations.....48

11. Acknowledgements 50

12. References.....51

13. Appendix.....56

1. Introduction

It has been known for more than a hundred years that CO_2 is a greenhouse gas and release of CO_2 from human activities may affect the climate on earth [1]. Power generation from fossil fuels is the largest source of global CO_2 emission. Several other sources such as oil refineries, petrochemical, steel and cement industry are also known to emit a substantial amount of CO_2. Further, a significant amount of CO_2 is released by the transportation sector [2]. CO_2 free power generation and reduced emission from the transportation sector will help considerably to solve the greenhouse problem. The idea of CO_2 capture and storage has received increased attention in the past few years. The CO_2 from a power plant can be captured and stored underground to reduce greenhouse gas emissions to the atmosphere. To capture CO_2 from a power plant, it needs to be separated from the flue gas stream. The technologies for CO_2 separation give substantial reduction in power plant efficiency and often need large equipment for separation [3]. Chemical-looping combustion (CLC) is a promising technology in which CO_2 is inherently separated from the rest of flue gases and therefore no extra energy or large equipment is needed for separation.

Hydrogen is a potential carbon-free fuel that may be used for both stationary power production and in the transportation sector. Production of hydrogen from natural gas gives rise to emissions of CO_2 to the atmosphere. There are limited options for the economical H_2 production without CO_2 emissions. Minor amounts of high-purity H_2 are produced from biomass and by electrolysis of water, where electricity is produced without CO_2 emissions. However, at present these options are not preferred because of high cost and some technical problems. Consequently, it is likely that the production of H_2 from steam reforming of natural gas will be a dominant technology in the next few decades. During production of H_2 from natural gas, an appreciable amount of CO_2 is released. Thus, in order for the process to become CO_2 free, the CO_2 has to be separated and stored. Steam reforming of natural gas needs severe operating conditions. The reformer operates at 800-850 °C and the reaction in the reformer is endothermic and hence a large quantity of fuel must be burnt in external burners to supply the energy necessary to maintain the high reformer temperature. To make the process CO_2 emission free, H_2 can be recycled from the process to the burners. However, about 30 % of the produced H_2 needs to be recycled to meet the energy demand [4]. This gives a decrease in efficiency of the process. Chemical-looping reforming (CLR) is an innovative technology, based on CLC, for production of hydrogen and power from natural gas with CO_2 capture.

In this thesis, new technologies for CO_2 capture from power plants and combined hydrogen and power production with CO_2 capture, namely CLC and CLR, are investigated. Both technologies use metal oxide as an oxygen carrier that transfers oxygen from air to the fuel. In the fuel reactor, fuel is oxidized by an oxygen carrier i.e. a metal oxide. The reduced metal oxide or metal is then transported to the air reactor, where it is oxidized by air into its original state, before it is returned again to the fuel reactor. In CLC, the products from the fuel reactor are only CO_2 and H_2O. Thus, pure CO_2 can be obtained by only condensing H_2O. In CLR, the product stream from the fuel reactor contains an undiluted mixture of H_2, CO, CO_2 and H_2O. This stream can then be transformed to only CO_2 and H_2 in a shift-reactor after which CO_2 and H_2 can be separated. Although several types of designs are possible, it is likely that interconnected-fluidized-bed reactors will be the most suitable reactor design for both technologies[5-8].

2. Objective

In order to make chemical-looping technologies successful, it is important to find promising oxygen carrier particles. In common to both technologies, the oxygen carrier particles need to have a combination of suitable properties, for instance high reaction rates, high mechanical strength and limited or no deactivation. For CLR, the particles should have high selectivity towards hydrogen formation. The objective of this work is to develop and evaluate some oxygen carrier for CLC and CLR with focus on reactivity and kinetics. Further, the reactivity data is used for preliminary design calculations for a real CLC system.

3. Background

The atmospheric concentration of CO_2 has been increased from 280 ppm to 370 ppm in the past century, which is mainly due to industrial activities. During the same time period the global average temperature has increased by approximately 0.6 °C [9]. Figure 1 shows the observed changes in global mean temperature in the past 140 years.

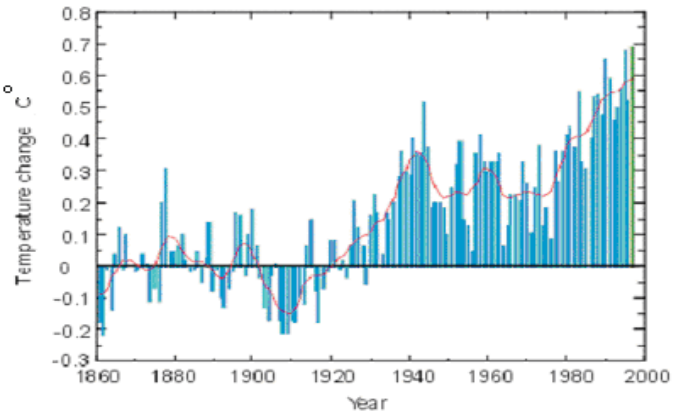

Figure 1 The observed change in global mean temperature at ground level [9] .

There is considerable evidence to suggest that the observed temperature increase has been caused by emission of greenhouse gases, of which CO_2 released from fossil fuel combustion is the primary one [1]. It is now generally accepted that there should be limits for concentrations of CO_2 and the other greenhouse gases in the atmosphere. One step towards limiting the emissions of greenhouse gases to the atmosphere was the implementation of the Kyoto protocol in 1997. According to this protocol, the developed countries agreed to reduce their emissions by 5.2% below the 1990 level in the period 2008-2012. Presently, the agreement has been ratified by 127 countries, the notable exceptions being USA and Australia, and came into force on 16 February 2005. If the Kyoto Protocol is fully implemented and successful, it is predicted to reduce the average global temperature by, given the widest range of estimates, between 0.02°C and 0.28°C by the year 2050. Since CO_2 is the main anthropogenic greenhouse gas, in order to meet the Kyoto agreement demands, a major reduction in CO_2 emission would be required.

Approximately 80% of the world's energy is produced by fossil fuel combustion [10]. CO_2 emissions can be reduced by using less energy by improving the energy efficiency and switching the fuel to renewable energy resources (e.g., biofuel, wind, solar and nuclear energy). The use of biofuel would need a large area for cultivation of biomass, which may conflict with other land uses such as food production. The future of nuclear power depends on public and political acceptance and the cost for building nuclear power plants is higher than fossil fuel power plants. Although the use of wind power is increasing rapidly and the future contribution from wind power is likely to be significant, the availibilty of suitable sites is expected to set an upper limit to its use. As compared to fossil fuels, solar power is very expensive today, although the cost is decreasing.

It is very likely that in the short to medium term energy needs will depend mostly on fossil fuels. One way to reduce CO_2 emissions from fossil fuels combustion is to separate CO_2 from the flue gas and subsequently store it. Main options for CO_2 storage are depleted oil and gas fields, deep saline aquifers, deep ocean and unmineable coal seams [11-13]. The details about different storage options can be found elsewhere [3].The global potentials for underground CO_2 storage, estimated by the IEA Greenhouse Gas R&D Programme, are shown in Table 1 [9]. These numbers may be compared with projected total emissions between 2000 and 2050, according to a "business as usual" scenario, which shows that this technique could have a substantial impact on CO_2 emissions.

Table 1 *Global capacity for CO_2 storage [9].*

Storage option	**Global capacity**	
	Gt CO_2	***% of emission to 2050***
Depleted oil and gas fields	920	45
Deep saline aquifers	400-10 000	20-500
Unminable coal beds	> 15	> 1

There are different techniques that can be used for CO_2 capture coming from combustion of fossil fuels, including post-combustion treatment, pre-combustion treatment and oxy-fuel firing. In post combustion treatment, amines are used for separation of CO_2 from the flue gas stream. In pre-combustion treatment, CO_2 is separated from the fuel before combustion and fuel is converted into hydrogen-rich fuel, which is then used for combustion. In the oxy-fuel technique, combustion is done with pure oxygen and thus an energy-intensive air separation unit is required. A common disadvantage with these techniques is the high cost for capture. A large amount of energy is required for CO_2 separation, which reduces the relative plant efficiency with about 7-12% [14]. It should be noted that about 75% of the total energy needed for CO_2 capture and storage comes from the separation of CO_2 from the rest of the flue gases.

This thesis describes new type of unmixed combustion technologies, CLC and CLR, where either power or hydrogen are produced and CO_2 is inherently separated from nitrogen and therefore no energy or gas separation equipment is needed for separation.

4. Chemical-looping technologies

4.1 Chemical-looping combustion

CLC is a combustion technique, in which CO_2 is inherently separated during combustion from the rest of the flue gases with only small energy losses. A metal oxide is used as an oxygen carrier to transfer oxygen from the combustion air to the fuel, which avoids direct contact between air and fuel [7, 15-17]. The process is composed of two fluidized reactors--an air and fuel reactor as shown in the Figure 2.

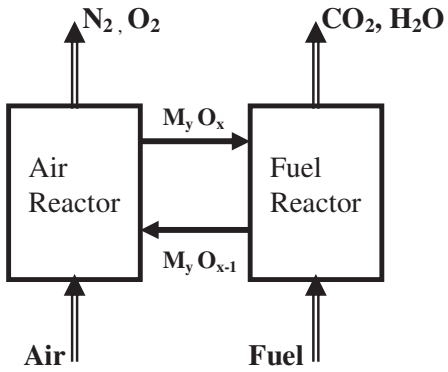

Figure 2 Chemical-looping combustion.

Fuel is introduced in gaseous form to the fuel reactor, where it is oxidized by the metal oxide (M_yO_x) according to:

$$(2n + m)\ M_yO_x + C_nH_{2m} \text{ ======> } (2n + m)\ M_yO_{x-1} + nCO_2 + mH_2O \qquad (1)$$

The outlet stream from the fuel reactor contains CO_2 and water, which means that by condensing the steam pure CO_2 can be obtained. The reduced metal oxide (M_yO_{x-1}) is then circulated to the air reactor where it reacts with air and is oxidized back according to:

$$M_yO_{x-1} + ½\ O_2 \text{ ======> } M_yO_x \qquad (2)$$

The flue gas stream leaving the air reactor will contain N_2 and some un-reacted O_2. The reaction between the fuel and metal oxide in the fuel reactor may be endothermic as well as exothermic depending on the metal oxide and fuel used, whereas reaction in the air reactor is always exothermic. The total amount of heat evolved in reaction 1 and 2 is the same as in the normal combustion. However, thermodynamic analysis showed that exergy destructions in CLC are lower than in the normal combustion, which increases the net power efficiency [15,

16]. The advantage with this system as compared with the normal combustion is that CO_2 and H_2O are inherently separated from the rest of the flue gases, and no energy is needed for separation. Thus in comparison with the other CO_2 separation techniques, CLC is potentially much cheaper. Further, no large size separation equipment is required. Because air and fuel go through different reactors and combustion takes place without flame, NOx formation should not be a problem [18].

4.1.1 CLC reactor design

A good contact is required between the gas and solid in CLC in addition to circulation of the oxygen carrier between air and the fuel reactor. It is likely that two interconnected fluidized bed will be the most suitable reactor design. A design based on two interconnected fluidized beds has been presented by Lyngfelt et al. (Figure 3) [7]. In the air reactor, or the riser, oxygen is transferred from combustion air to the oxygen carrier and in the fuel reactor oxygen is transferred from oxygen carrier to fuel. The volumetric gas flow in the air reactor is considerably higher than that of the gaseous fuel. To prevent gas leakage between the two reactors, conventional loop seals can be used. The exit stream from fuel reactor is condensed to remove water, and the remaining gas containing mostly CO_2, is compressed and cooled in stages to yield liquid CO_2. The remaining non-condensable combustible gases may be recycled to the fuel reactor or burnt with the addition of some oxygen downstream the fuel reactor is also an option. Johansson et al. constructed a cold-flow model with a design similar to that in Figure 3 and explored suitable operating conditions for achieving a sufficient solids flux of particles between the reactors and solids inventory in the reactors [19]. Further, leakage between the reactors was low as long as proper pressure differences within the system were maintained [20]. Kronberger et al. [21] conducted tests on a cold-flow model of a chemical-looping combustor with the principal layout shown in Figure 3. Stable and suitable operating conditions were identified.

Several CLC prototypes have been presented in the literature. Lyngfelt et al. presented results from a 10 kW prototype unit [6, 22]. Here, an oxygen-carrier based on nickel oxide

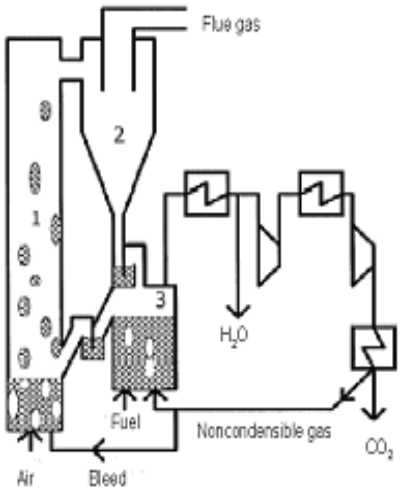

Figure 3 Layout of chemical-looping combustion process, with two interconnected fluidized beds. 1) Air reactor 2) Cyclone 3) Fuel reactor [7].

was operated for 100 h using natural gas as fuel. A fuel conversion efficiency of 99.5% was achieved, and no carbon dioxide escaped to the air reactor. Thus, all carbon dioxide was captured in the process and only small losses of fines were observed. Ryu et al. have presented results from a 50 kW combustor operating with methane as fuel, and two types of oxygen-carriers [8]. A nickel oxide oxygen-carrier was tested during 3.5 h and a cobalt oxide was tested during 25 h. For the nickel oxide oxygen-carrier, the concentration based on dry flue gases of CO_2 leaving the fuel reactor was 98% and for cobalt oxide 97%. The two reactors have a similar design, but differ at the return from the fuel reactor. In the 10 kW unit at Chalmers the particles leave the fuel reactor through an overflow, i.e. the bed height in the fuel reactor is always constant, whereas in the 50 kW unit in South Korea the particles leave the fuel reactor from the bottom of the bed, and the particle flow i.e. the bed height of the fuel reactor, is controlled by a valve. Adanez et al. [5] have also presented a 10 kW CLC unit that was operated for 120 h using a CuO-based oxygen carrier of two particle sizes. Finally, oxygen carriers based on Ni, Mn and Fe have been used in a 300 W CLC reactor with both syngas and natural gas [23-27]. This reactor was designed specifically for testing smaller amounts of oxygen carrier material in a continuous fashion and was based on a cold-flow model tested by Kronberger et al [28].

4.2 Chemical-looping reforming

CLC can be adapted for H_2 production with some modification. The idea of using CLC for H_2 production was first presented by Mattisson and co-workers [29, 30]. Ryden and Lyngfelt have conducted investigations of various systems incorporating CLR and found efficiencies of 73-81% based on the lower heating value of natural gas, depending if the process is atmospheric or pressurized [31-33]. They also investigated Ni-based oxygen carrier specifically for CLR in a 300W continuous reactor with promising results [27]. The main difference between CLR and ordinary CLC is that fuel is partially oxidized in CLR. A simple schematic diagram of integrated H_2 and power production process or CLR is shown in Figure 4.

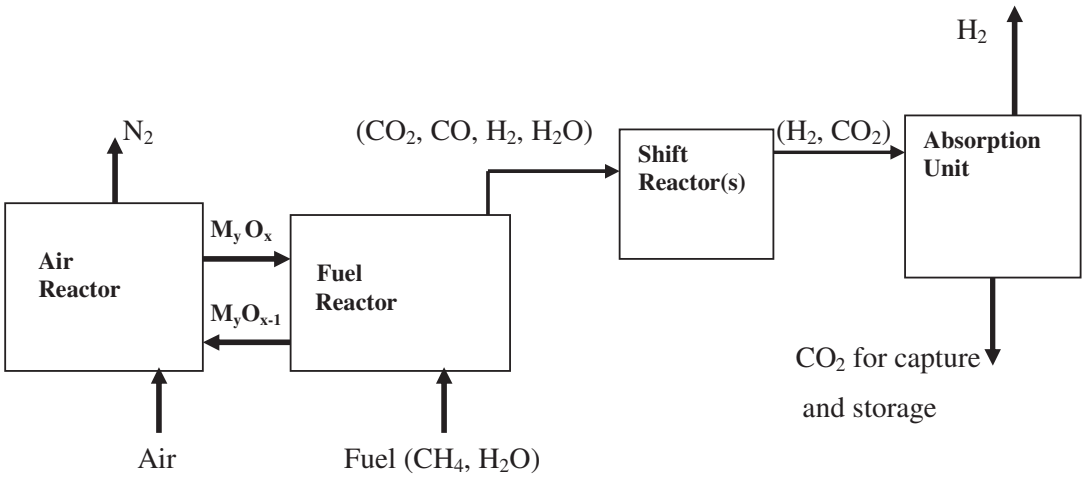

Figure 4 Simple flow diagram of chemical-looping reforming.

In the fuel reactor, water and fuel (CH_4 in this case) reduce the metal oxide (M_yO_x) to a lower oxidation state (M_yO_{x-1}) forming a mixture of CO_2, CO, H_2 and H_2O. The product stream from the fuel reactor is sent to shift reactor, where CO and H_2O will react via:

$$CO + H_2O \quad ======> \quad CO_2 + H_2 \qquad (3)$$

Thus a stream composed mainly of H_2 and CO_2 will be obtained. H_2 and CO_2 can be separated by physical or chemical absorption, and depend upon the H_2 purity required as well as the pressure. The reduced metal oxide (M_yO_{x-1}) is transferred to the air reactor, where it reacts with air according to reaction 2 and is oxidized back to its original form (M_yO_x).

4.3 Oxygen carriers

Most of the work concerning the development and characterization of oxygen carriers is related to CLC. The oxygen carrier is generally composed of a metal oxide (active phase) and support (inert phase). The inert phase acts as a porous support providing a higher surface area for the reaction and increased mechanical strength of the particles. In regular CLC, the oxygen carrier should be able to convert the fuel gas completely to CO_2 and H_2O in the fuel reactor. Mattisson and Lyngfelt showed that the possible yield of methane to CO_2 and H_2O was a function of the metal oxide used as well as the temperature [34] . This restriction will not be applicable to CLR because full conversion of the fuel gas to CO_2 and H_2O in the fuel reactor is not desired. Thus metal oxide systems such as Fe_3O_4/FeO and CoO/Co, which have lower degrees of conversion are not viable for CLC but may be more interesting for CLR.

In addition, oxygen carriers for both CLC and CLR should have the following properties:

- High reactivity during reduction by fuel gas and oxidation by air.
- The particles should be resistant towards carbon formation.
- The particles should have enough mechanical strength to bear the stresses resulting from circulation of the particles between the two reactors.
- The particles should be resistant towards agglomeration.
- The particles should be cheap to produce and in an environmentally sound way.
- The cost of production should be low.

Oxygen carriers investigated so far in literature are primarily based on Fe, Cu, Co, Mn and Ni. There are a number of research groups around the world working on oxygen carrier development. A short summary of the main contributors follows below:

Ishida and co-workers at the Tokyo institute of Technology in Japan investigated metal oxides of Fe, Ni and Co with Al_2O_3, TiO_2, MgO, $NiAl_2O_4$ and YSZ (yttria stabilized zirconia) as inert support and using H_2, CO and CH_4 as fuel in a thermogravimetric analyzer (TGA). They have investigated the effect of temperature, gas composition and particle size on the reduction and oxidation rates as well as the carbon deposition characteristics of the oxygen carrier particles [35-48]. Limited work has also been done in a fixed bed [49] and in a continuous reactor [50]. Of the many oxygen carriers investigated by this group, in general Ni-based oxygen carriers showed the best promise. Among these, NiO/$NiAl_2O_4$ was identified as an excellent oxygen carrier for CLC [46].

Copeland and co-workers at TDA Research Inc. investigated Ni-, Fe- and Cu-based oxygen carriers using H_2 and syngas as the fuel. They rejected CuO due to agglomeration problems [51-53].

Mattisson and co-workers at Chalmers University of Technology Sweden, investigated Fe_2O_3, Mn_2O_3, NiO, and CuO on Al_2O_3, SiO_2, $MgAl_2O_4$ and Mg-ZrO_2 supports in batch and continuous laboratory fluidized bed reactors and TGA using CH_4 and syngas as fuel both for CLC and CLR [29-31, 34, 54-74] They have found that the sintering temperature has a strong effect on the structure and the reactivity of particles [60]. NiO/$MgAl_2O_4$ was found to be a promising oxygen carrier both for CLC and CLR [25, 27, 74] whereas Mn_3O_4/Mg-ZrO_2 showed excellent reactivity for CLC without any signs of agglomeration [24, 58, 64]. Cho et al. investigated carbon formation on Ni- and Fe-containing oxygen carriers and found that for Ni-carriers a significant amount of carbon is formed when 80% of the available oxygen is consumed in the particles, whereas no carbon was formed on Fe-carriers [57]. Ni-based particles were also used in a 10 kW reactor for 100 h operation A high conversion of fuel was observed without any agglomeration of particles [6, 22]. A detailed review of work done on oxygen carriers can be found in Mattisson et al. [75].

Ryu and co-workers at the Korea Institute of Energy Research studied the effect of metal oxide content in an oxygen carrier and reaction temperature on reactivity of NiO/bentonite particles and found 900˚C is a suitable temperature to achieve reactivity and avoidance for carbon deposition [76, 77]. Further, Ni- and Co-based oxygen carriers were used in a 50 kW prototype based on interconnected fluidized beds. Here no NOx formation was observed [8, 78] .

Villa and co-workers at Dipartimento di Chimica, Italy investigated NiO on $NiAl_2O_4$ and $MgAl_2O_4$ as supports using methane as fuel. The results indicated that investigated oxygen carriers have high selectivity toward H_2 and CO. Further the presence of $NiAl_2O_4$ spinel prevents the crystal size growth of NiO and addition of Mg limits the sintering of the cubic NiO [79].

Adanez and co-workers at Instituto de Carboquimica (CSIC), Zaragoza Spain investigated oxides of Cu, Ni, Mn, and Fe supported on Al_2O_3, SiO_2, sepiolite, TiO_2 and ZrO_2 [5, 80-88]. They concluded that SiO_2, Al_2O_3, ZrO_2 and TiO_2 are promising support materials for CuO, Fe_2O_3, Mn_3O_4 and NiO respectively [81] and for Cu-based oxygen carriers, impregnation on a support is an excellent preparation method for obtaining high crushing strength and high redox reactivity [85]. Garcia-Labiano et al. studied the kinetics of reduction and oxidation of CuO (10%) impregnated on alumina using CH_4, H_2 and CO as fuel gas and O_2 as oxidizing gas in a TGA. The metal oxide reacted with the fuel with reactivity rates in order H_2 > CO >CH_4 [87]. The authors also studied the theoretical temperature variations in the oxygen carrier particle during reduction and oxidation and found that for a typical CLC system, maximum temperature of particles is highly dependent on particle size, overall reaction time and the resistance to heat transfer in external gas film, whereas less dependent on oxygen carrier porosity, activation energy, type of inert material and metal oxide fraction in the carrier [88].

Corbella and co-workers at Instituto de Catalisis Petroleoquimica Madrid Spain, investigated NiO, CuO supported on TiO_2 and SiO_2 prepared by wet impregnation using CH_4 as fuel in a fixed bed reactor [89-92] . The findings showed that the reactivity of nickel-based oxygen carriers was independent of Ni loading [90]. In case of CuO/TiO_2 the active metal

does not interact with the support. However copper was redistributed in the support, promoting a more uniform distribution that decreases the pore volume but not the carrier performance [89]. CuO/SiO_2 showed a stable reactivity and no redistribution of copper was observed on SiO_2 support because of the lower temperature used in the experiments [91].

Stobbe investigated reduction and oxidation behaviour of unsupported manganese oxides using CH_4 and O_2 for a process similar to CLC and CLR. It was found that the reduction rate of manganese oxides is mainly determined by their crystallinity [93].

It is somewhat difficult to compare the results of the different oxygen carriers from the above review. This is because reactivity data are very much dependent on type and loading of metal oxide, method of preparation and fuel gas as well as the reactor type used in the investigation. However, it can generally be concluded that nickel- and copper-based materials are the most reactive using methane as fuel. Copper based oxygen carriers have shown agglomeration tendencies in several studies but copper oxygen carriers prepared by impregnation have shown high reactivity with no agglomeration [5, 85]. Mn- and Fe-based oxygen carriers are generally reduced faster when H_2 and CO are used as fuel as compared with methane [23, 94]. The reaction rate increases as reactant gas concentration and reaction temperature increases and is independent of the particle size.

In the present work oxygen carriers based on Ni, Cu, Mn and Fe were investigated in a laboratory fluidized-bed reactor and a TGA using methane as fuel. Three types of supports were used, i.e. SiO_2, $MgAl_2O_4$ and $Mg\text{-}ZrO_2$. It was found that Ni-based oxygen carriers are promising for CLR, whereas Cu-, Fe- and Mn-based oxygen carriers have poor selectivity towards hydrogen formation and thus are not suitable for CLR. Moreover, reduction and oxidation kinetics of two promising oxygen carriers, $NiO/MgAl_2O_4$ and $Mn_3O_4/Mg\text{-}ZrO_2$ for CLC are determined. Kinetic data has a great importance in the design of a CLC system, because it is related to the amount of oxygen carrier material needed in the air and fuel reactors to transfer the oxygen demanded by combustion of the fuel gas.

5. Experimental work

5.1 Preparation of oxygen carriers

Particles investigated in this work were prepared by dry-impregnation and freeze granulation methods. Oxygen carriers investigated for CLR were prepared by impregnation; while oxygen carriers used for CLC kinetic determination were prepared by freeze granulation. The reason for choosing the impregnation method is that this is used to produce catalyst particles on industrial scale. Freeze-granulation is generally used to produce small batches of particles but is rather similar to the spray drying which is a method for producing particles on industrial scale.

5.1.1 Impregnation

Oxygen carriers of iron, manganese, copper and nickel on SiO_2 and $MgAl_2O_4$ were prepared by dry-impregnation. The commercial support particles of SiO_2 (Sipernat 2200, Degussa AG) and freeze granulation particles of $MgAl_2O_4$ were heated at 250 ℃ for 2 h to evaporate moisture completely. These particles were then exposed to a warm (60 ℃) and highly concentrated aqueous solutions of metal nitrates (Table 2). A volume of metal nitrate solution corresponding to the pore volume of SiO_2 and $MgAl_2O_4$ was added to each sample. The oxygen carriers were dried at 110 ℃ for 3 h to remove pore water, followed by calcination at 500 ℃ for 3 h to remove NO_2 and form metal oxides.
With the exception of CuO/SiO_2 all samples were sintered for 6 h at 950 °C. The CuO/SiO_2 particles were sintered at 800 ℃. The reason for the lower sintering temperature is the lower melting point of Cu, which is 1083 ℃. Finally oxygen carriers were sieved to get different particle size ranges of 180-250, 125-180 and 90-125 μm.

Table 2 *Metal nitrates used for impregnation*

Metal nitrate	Formula	Manufacturer
Nickel nitrate	$Ni(NO_3)_2.6H_2O$	Scharlau Chemie S.A Barcelona Spain
Iron nitrate	$Fe(NO_3)_3.9H_2O$	Scharlau Chemie S.A Barcelona Spain
Copper nitrate	$Cu(NO_3)_2.3H_2O$	Scharlau Chemie S.A Barcelona Spain
Manganese nitrate	$Mn(NO_3)_2$. x H_2O	Sigma Aldrich Chemie GmbH Germany

5.1.2 Freeze granulation

The particles investigated for CLC were $NiO/MgAl_2O_4$ and $Mn_3O_4/Mg\text{-}ZrO_2$, which were prepared by freeze granulation. In freeze granulation commercial metal oxide powder and inert material (< 10 μm) were mixed with distilled water and a small amount of polyacrylic acid was added as dispersant. The mixture was grinded in ball mill for 24 h and a small amount of polyvinyl alcohol was added as binder to hold the particles intact during freeze drying and sintering. The resulting slurry was pumped to a spray nozzle, where atomizing air produce drops of slurry. These drops were sprayed into the liquid N_2, where they froze instantaneously. The water in the particles was removed by sublimation in a freeze dryer operating at a pressure that corresponds to the vapour pressure over ice at -10 °C. After drying Ni-based and Mn-based particles were sintered at 1400 °C and 1150 °C respectively, for 6 h. The particles were then sieved to get different size range. Metal loadings and BET surface area of the oxygen carriers used in this work are shown in Table 3. It can be seen that particle

produced by impregnation have higher BET surface area compared with freeze-granulated particles. This may be due to the higher sintering temperature used for preparation of particles with the freeze-granulation method. It should be noted that depending on the temperature, manganese oxide may contain either Mn_2O_3 or Mn_3O_4. The general transition temperatures for manganese oxides are the following

$$MnO_2 \xrightarrow{500°C} Mn_2O_3 \xrightarrow{900°C} Mn_3O_4 \xrightarrow{1700°C} MnO \quad (4)$$

It was found that Mn_2O_3 was the phase when SiO_2 was used as a support. However, thermodynamically Mn_3O_4 is the stable manganese phase at 950 ℃ in air but it could not be identified and only Mn_2O_3 was found in the fresh sample (Table 5). In this work different ratios of manganese oxide to inert material are used for the preparation of oxygen carrier particles and therefore particles may have different properties than pure manganese oxide at different temperatures. A discussion about the different manganese oxide phases at different temperatures can be found in attached paper IV.

Table 3 O*xygen carriers used in this work*

Oxygen Carrier	MeO (wt %)	Sintering Temperature (℃)	BET (m^2/g)
NiO/SiO_2	34.5	950	39.7
Fe_2O_3/SiO_2	39.4	950	46.7
CuO/SiO_2	41.3	800	70.2
Mn_2O_3/SiO_2	47.0	950	11.6
$NiO/MgAl_2O_4$	36.5	950	5.2
$Fe_2O_3/MgAl_2O_4$	31.8	950	4.4
$Mn_2O_3/MgAl_2O_4$	46.0	950	3.2
$CuO/MgAl_2O_4$	43.0	950	2.6
$NiO/MgAl_2O_4$*	60.0	1400	3.0
$Mn_3O_4/Mg\text{-}ZrO_2$*	40.0	1150	1.2

* prepared by freeze granulation method

5.2 Characterization of oxygen carriers

All the oxygen carriers were characterized before and after the experiment. Shape and morphology of fresh and reacted oxygen carriers were studied using scanning electron microscope (ESEM, Electroscan 2020, ULTRA 55- LEO and JEOL JSM 5200). To see what kind of chemical changes occurred in the oxygen carrier particles during the redox experiments, all oxygen carriers were characterized using x-ray powder diffraction (Siemens D5000 Powder Diffractometer utilizing Cu K_α radiations).
BET surface area of fresh particles was measured, using an ASAP 2010 instrument (Micrometrics). The force needed to break the particle was measured with a crushing strength apparatus Shimpo FGN-5. The crushing strength was measured on particles in the size range 180-250 μm.

5.3 Experimental methods

Two kinds of experimental methods are used in this work for determining the reactivity of oxygen carriers: fluidized bed and TGA. In fluidized-bed experiments the oxygen carrier

particles are exposed to environment, which better simulates the conditions in a real system. It is also possible to measure the outlet gas concentration from the reactor and thus the selectivity to the different gaseous products. However, a relatively large amount of material is needed in this method i.e. 10-15 g. This amount of bed material was reasonable to obtain a good measure of the reaction with the method. But also because the oxidation rate is often relatively high, this means that all incoming oxygen reacts with the oxygen carrier particles. Thus, it is not possible to measure a rate of reaction, which is not limited by the supply of oxygen in the same experiment. However; this is not the case in the TGA where a very small amount of material is needed in TGA experiments i.e. 20-100 mg. In addition, in TGA experiments, there are no complicated fluidizing effects and it is a good method for the determination of reaction kinetics.

5.4 Experiments in laboratory fluidized bed reactor

The experimental setup for the reactivity investigation with the fluidized bed reactor is shown in Figure 5. A fluidized-bed reactor made of quartz was used for the experiments. The reactor had a length of 820 mm with a porous quartz plate of 30 mm in diameter placed at a distance of 370 mm from the bottom. The inner diameters of top and bottom sections were 30 and 19 mm respectively. Temperatures were measured 5 mm below and 10 mm above the porous quartz plate using 10% Pt/Rh thermocouples enclosed in quartz shells. The pressure drop over the bed was measured during the experiment. NiO, CuO, Fe_2O_3 and Mn_2O_3 supported on SiO_2 were tested in the fluidized bed reactor using alternating oxidizing and reducing atmospheres at different temperatures (700-950 °C).

A sample of 10 or 15 g of oxygen carrier in a size range from 180-250 μm, was heated to the desired temperature in an inert atmosphere (N_2). The bed height varied in a range between 20 and 35 mm because of the difference in apparent densities of the various oxygen carriers. The oxygen carrier particles were then exposed in an alternating sequence to 5% O_2 in nitrogen during the oxidation period and 50 % CH_4 and 50 % H_2O during the reduction period. Depending upon the oxygen carrier used in the experiment, the reduction period varied between 100 and 400 s and the oxidation period varied between 1000 and 3600 s. Nitrogen was introduced for 180 s after each oxidation and reduction periods to avoid mixing between CH_4 and air. All particles were tested in the reactor for 4-7 cycles.

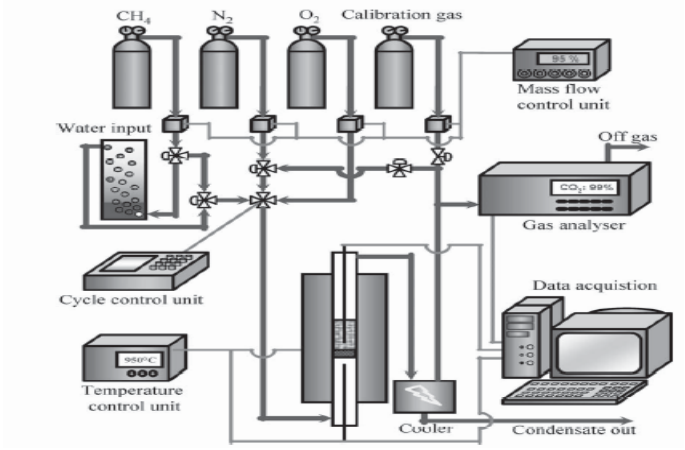

Figure 5 Fluidized bed reactor experimental setup [57].

Flow rates used for oxidation, reduction and inert periods were 600 mL/min (at 1bar and 0°C) in the experiments conducted with 10 g bed mass; for 15 g bed mass, the gas flow was 900 mL/min. In this way, the ratio of the volume flow to bed mass was kept constant. These flows correspond to 4-8u_{mf} and 6-11u_{mf} for the incoming reducing and oxidizing gas respectively, where u_{mf} is the minimum fluidization velocity [95]. The oxidation reaction is highly exothermic and thus a temperature increase is likely in the bed during oxidation. In this type of laboratory setup it is not possible to cool the reactor. Thus, to limit this increase, the oxygen concentration used was only 5%. The gas from the reactor was led to an electric cooler, where the water was condensed and removed. Then the gas was passed through a gas analyzer (Rosemount NGA-2000) where the concentrations of CO_2, CH_4, CO and O_2 were measured in addition to the gas flow. The concentration of H_2 was not measured during the reduction but was assumed to be equal to the difference 1-(x_{CH4} + x_{CO2}+ x_{CO}) where x_i is the outlet volume fraction of gaseous component i after removal of water. However, because of back mixing in the system, the H_2 concentration in the initial part of period was calculated by assuming that the hydrogen concentration could be predicted through equilibrium of the water-shift reaction. From a mass balance and from the equilibrium constraint, the H_2 partial pressure was calculated from,

$$p_{H2}= 3K*p_{CO,out}\,(p_{CO2,out} + p_{CO,out} +1/3*p_{CH4,out})/(p_{CO2,out} + K*p_{CO,out}) \qquad (5)$$

where K is equilibrium constant for water-shift reaction at a given temperature and $p_{CO2,out}$, $p_{CO,out}$ and $p_{CH4,out}$ are the partial pressures of outgoing CO_2, CO and CH_4 respectively after the removal of water.

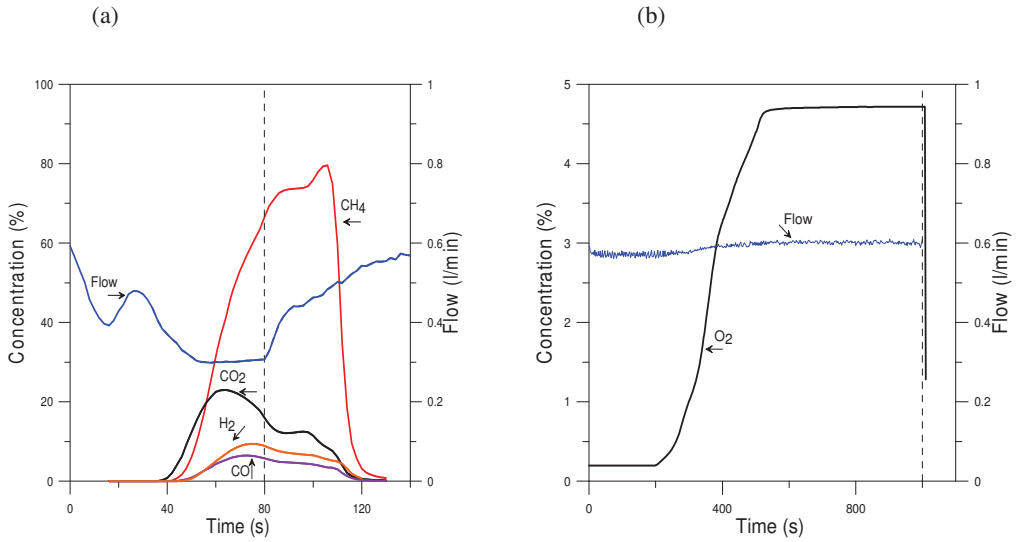

Figure 6 Outlet gas concentration from the fluidized bed reactor for the reactivity experiment with Fe_2O_3/SiO_2 (a) 2nd reduction period (b) 3rd oxidation period. The vertical dashed line indicates the switch to inert atmosphere.

A typical concentration profile of the outlet gas concentrations for a reduction period is shown in Figure 6. In this case Fe_2O_3/SiO_2 particles initially react with incoming methane to form CO_2 (and water). In this case the CO_2 concentration reaches a maximum of approximately 25% about 70 s in to the reduction period. The reason for the long time between switching to the reducing atmosphere and the maximum reaction rate (i.e. the highest CO_2 concentration) is the delay time between the reactor and gas analyzer and back mixing, i.e. the product gases

mix with the nitrogen introduced before the reduction period. As the oxygen content in the particles decreases, the formation of H_2 and CO occurs as well as the release of methane. Concerning the gas flow seen in Figure 6a, it should be noted that the gas flow is measured in connection to the gas analysis, with flow variations upstream of the analysers rapidly affecting the measured flow, whereas changes in gas concentrations have to reach the analysers before being recorded. The gas flow will increase in the reactor during the reduction because of the formation of 3 moles product gas from each mole of methane at full conversion, see equation 1. Because the gas conversion varies with time, so will the flow. There is also a decrease in the gas flow in the condenser due to removal of water.

In the oxidation period, shown in Figure 6b the reaction rate is initially fast and all the incoming oxygen reacts with the oxygen carrier during the first 200 s and then reaction slows down with most of the O_2 released without reacting. The measured flow from the reactor during the initial part of oxidation is a little less (Figure 6b) because all oxygen entering the reactor is consumed by the particles in the beginning.

5.5 Experiments in thermogravimetric analyzer (TGA)

Most of the work in this thesis was done performing the experiments in TGA. In paper II Setaram TAG 24S16, TGA was used and the experimental setup is shown in Figure 7.

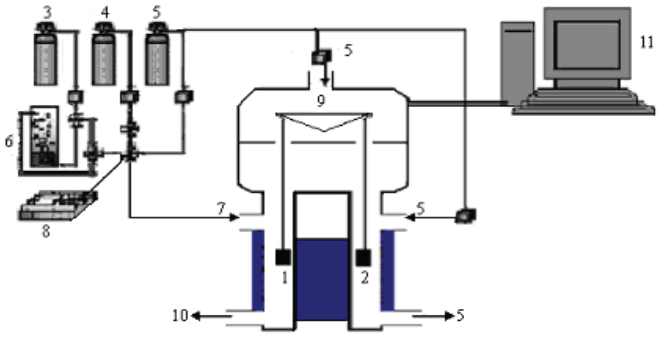

Figure 7 The Setaram TAG 25S16 TGA experimental set up. **1=** Furnace 1 with sample**, 2=**Furnace 2**, 3=**Fuel gas**, 4=**O_2**, 5=**N_2**, 6=**Water**, 7=** Reaction gas entering the reactor**, 8=**Cycle control unit**, 9=**Microbalance**, 10=** Outlet gases from reactor**, 11=** Data collection

This TGA uses a double furnace system and permits compensation for any perturbation resulting from gas flow and buoyancy effects. The details about the experimental procedure can be found in paper II.

The kinetic investigation of some promising oxygen carriers was done (paper III and IV) by performing the experiments in a high-resolution TGA (TGA 2950, TA Instruments). The reactor was an evolved gas analysis (EGA) furnace consisting of a quartz tube (15mm ID) and the sample holder was a platinum pan (9 mm ID).

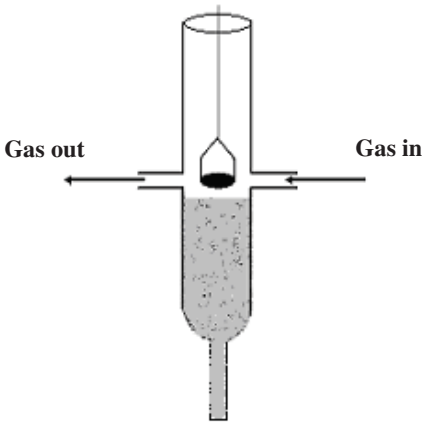

Figure 8: Furnace in the TGA 2950, TA Instruments

The reacting gas enters from one side of the quartz tube, reacts with the sample and leaves the tube from the other side as shown in Figure 8. The lower part was filled with inert quartz particles to reduce the volume of the reactor tube. A 20 mg oxygen carrier sample was heated in the platinum pan to the desired reaction temperature (800-1000°C) in a nitrogen atmosphere. The particles were well spread in the platinum pan forming a single layer, in order to avoid the inter-particle mass transfer resistance. The sample was exposed in cyclic manner to a reducing gas between 5 and 25% CH_4 and 20% H_2O balanced with N_2 for the reduction period and to an oxidizing gas between 3 and 15% O_2 balanced with N_2 for the oxidation period. The CH_4 and O_2 concentrations used in the experiments are in the range of the average gas concentration, which the particles may be exposed to in the fuel and air reactors. The steam was added during reduction period to avoid any carbon formation on the particles but also to better simulate the environment to which the particles are exposed to in the fuel reactor. Depending on the reaction temperature and reacting gas concentration used in the experiment, the reduction period was 50-140 s and oxidation period was 70-150 s long. N_2 was introduced for 200 s after each reducing and oxidizing period to avoid mixing between methane and oxygen.

The flow of the gas into the reactor was controlled by electronic mass flow regulators and was 300 mL/min (normalized to 1 bar and 0°C) for all the periods and cycles. 10% of the total gas flow (i.e. 30 mL/min purge N_2) was always introduced from the head of the TGA to keep the balance parts free from any corrosive gas. Some tests were performed with different gas flows and no effect on reaction rate was observed. It was thus concluded that mass transfer resistance is not rate limiting in these experiments. However, in the initial part of the reaction the reaction rate increased for 3-5 s, depending on the temperature and the gas concentration used in the experiment. This is likely due to some small back-mixing in the system and thus there is a short time when the methane concentration is lower than the desired concentration. In the experiments the gas flow was relatively high and the reactor volume small. Accordingly calculations showed that the gas residence time in the reactor should be less than 0.5 s. Because of this short delay time, the measured reactivity data for the first few seconds were not used in the calculations, but instead the rate was extrapolated from data obtained when there was no back-mixing. At least four cycles of reduction and oxidation were performed for each experiment. Generally, the first cycle was less reactive than the preceding cycles, which was likely because of the internal restructuring inside the particle.

5.6 Data evaluation

The degree of oxidation or conversion is defined as,

$$X = (m-m_{red}) / (m_{ox}-m_{red}) \quad (6)$$

where m is the actual mass of the sample, m_{ox} is the mass of the sample when it is fully oxidized and m_{red} is the mass of fully reduced sample.
For fluidized bed reactor experiments, the degree of conversion in reducing period was calculated as a function of time through,

$$X_i = X_{i-1} - \int_{t_0}^{t1} \left(1/ (M_o*P_{tot})\right) n_{out} \left(4p_{CO2,out} + 3p_{CO,out} - p_{H2,out}\right)dt \quad (7)$$

and for oxidizing period was calculated from,

$$X_i = X_{i-1} + \int_{t_0}^{t1} \left(2/(M_o*P_{tot})\right) \left(n_{in}p_{O2,in} - n_{out}p_{O2,out}\right) dt \quad (8)$$

where X_i is the conversion as a function of time for period i, X_{i-1} is the conversion after the preceding period, t_0 and t_1 are the times for start and end of the period respectively, M_o is the moles of active oxygen in the fresh oxygen carrier, n_{in} and n_{out} are the molar flow rates of the gas entering and leaving the reactor after the water has been removed, P_{tot} is the total pressure and $p_{O2,in}$, $p_{O2,out}$, $p_{CO2,out}$, $p_{CO,out}$ and $p_{H2,out}$ are the partial pressures of incoming and outgoing O_2 and outgoing partial pressures of CO_2, CO and H_2 after the removal of water.
The rate of reduction of metal was based on the conversion of incoming methane and calculated from,

$$dX/dt = \left(1/(M_o*P_{tot})\right) n_{in,CH4} \left(4p_{CO2,out} + 3p_{CO,out} - p_{H2,out}\right) \quad (9)$$

where $n_{in,CH4}$ is the incoming molar flow rate of methane to the reactor. In the present work different oxygen carriers were compared. As inherently these have different mass fraction of active oxygen that can be transferred, in addition to the different metal oxide loadings, the oxygen carriers were also compared on mass basis using mass-based conversion, calculated from,

$$\omega = m/m_{ox} = 1 + R_o(X - 1) \quad (10)$$

where R_o is the oxygen ratio defined as,

$$R_o = (m_{ox} - m_{red}) / m_{ox} \quad (11)$$

R_o is the maximum fraction of oxygen that can be transferred between air and fuel reactor. Oxygen ratios for different metal oxides and oxygen carriers used in this work are given in Table 4. The mass-based reduction rate was calculated from,

$$d\omega/dt = R_o \, dX/dt \quad (12)$$

Table 4 *Oxygen ratios of different metal oxides.*

M_xO_y/ M_xO_{y-1}	R_o
NiO/Ni	0.21
Fe_2O_3/ Fe_3O_4	0.03
CuO/Cu	0.20
Mn_3O_4/MnO	0.07

In contrast to CLC it is not of interest to reach full conversion to the oxidation products CO_2 and H_2O in CLR, i.e. the oxygen supplied from metal oxide and steam should be limited. To asses the amount of oxygen supplied during the reduction, the oxygen supplied ratio was defined as the amount of oxygen supplied from added H_2O and metal oxide divided by the amount of oxygen needed for final conversion to CO_2 and H_2. If 1 kmol/s CH_4 and z kmol/s H_2O are added to the inlet of the reactor from mass balance oxygen supplied ratio, o, can be calculated as,

$$o = [(4x_{CO2} + 3x_{CO} - x_{H2}) + z\,(x_{CH4} + x_{CO2} + x_{CO})]/\,[2(x_{CH4} + x_{CO2} + x_{CO})] \quad (13)$$

Thus if o is above unity it means excess of oxygen has been supplied as compared with that required for complete conversion to CO_2 and H_2 and on the other hand if o is below unity less oxygen has been supplied as compared with the required amount. In the latter case it would be necessary to supply more oxygen in later stages, perhaps excess steam to the shift reactor.

For TGA experiments in paper III and IV, the degree of conversion for reduction and oxidation was calculated as,

$$X_{red} = 1 - [(m-m_{red})/(m_{ox}-m_{red})] \quad (14)$$

$$X_{ox} = (m-m_{red})/(m_{ox}-m_{red}) \quad (15)$$

6. Gas-solid reaction models

Gas-solid reaction has large applications in the industrial process (e.g. roasting and reduction of ores, combustion of solids, coal gasification and sulfur capture). In CLC the reaction of fuel gas (e.g. CH_4 or H_2) with oxygen carrier particles is a non-catalytic type of solid-gas reaction. Several models for non-catalytic gas-solid reaction have been presented in the literature including the shrinking-core model (SCM), volume reaction model, grain model, pore model and cracking-core model [96-101]. However, the SCM is a simple and commonly used model [37, 102, 103].

In SCM, it is speculated that the reaction occurs first at the outer skin of the particle and then proceeds towards the centre of the particle and finally the particle is fully converted in which inert solid remains (Figure 9).

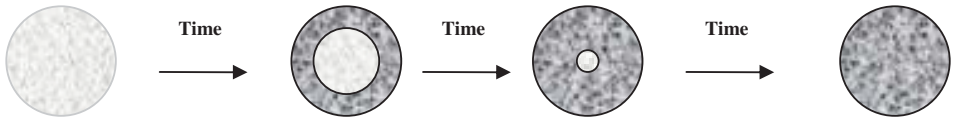

Figure 9: Reaction proceeding via shrinking-core model.

It is assumed that the particle size is unchanged and the unreacted core shrinks during the reaction until no reactant is left in the particle.

In the SCM there are five steps during reaction

- The reactant gas diffuses through the film surrounding the particle and reaches the surface of the particle.
- The reactant gas diffuses and penetrates through the product layer to reach the unreacted core of the particle.
- Reaction of gas with the reactant at the solid surface.
- Diffusion of the product gases through the product layer back to the exterior surface of the particle.
- Diffusion of the product gases through the gas film to the bulk.

The reaction may be controlled by one or all the resistance namely, gas film diffusion, diffusion though product layer and chemical reaction at the surface of the particle [101]. The equation of model when diffusion through gas film controls the reaction rate is

$$\frac{t}{\tau} = X \qquad (16)$$

where τ is the time for complete conversion and can be calculated from

$$\tau = \frac{\rho_m r_g}{3bkC_g{}^n} \quad (17)$$

The equation of model when diffusion through the product layer controls the reaction rate is

$$\frac{t}{\tau} = 1 - 3(1-X)^{2/3} + 2(1-X) \quad (18)$$

Here τ can be calculated from

$$\tau = \frac{\rho_m r_g{}^2}{6bD_e C_g{}^n} \quad (19)$$

When chemical reaction is controlling the rate of reaction, the equation of model is

$$\frac{t}{\tau} = 1 - (1-X)^{1/3} \quad (20)$$

and τ can be calculated from

$$\tau = \frac{\rho_m r_g}{bkC_g{}^n} \quad (21)$$

which can also be re-written as

$$\ln\left[\frac{\rho_m r_g}{b\tau}\right] = \ln(k) + n\ln C_g \quad (22)$$

Some work has been done in the literature regarding kinetics of oxygen carriers for CLC where the SCM model is most often used to predict the results. Ishida et al. studied the kinetics of NiO/YSZ particles prepared by the dissolution method and used the unreacted SCM to interpret the experimental results. It was concluded that reduction reaction with hydrogen is controlled by chemical reaction resistance, whereas oxidation is the intermediate reaction between chemical reaction and ash-layer diffusion. The activation energy was 82 kJ/mol for the reduction reaction and between 17 and 56 kJ/mol for the reaction with air [37]. Ryu et al. studied kinetics of NiO/bentonite and used the unreacted SCM to interpret the reduction and oxidation reaction. In this later study the fuel gas was methane and the oxidizing gas was oxygen. The authors concluded that the reduction reaction was controlled by chemical reaction, whereas the oxidation reaction was controlled by product layer diffusion [77]. The activation energies for reduction and oxidation reaction were about 9 and 31 kJ/mol respectively. Garcia-Labiano and co-workers determined the kinetics of reduction with CH_4, CO and H_2 and of oxidation with O_2 for oxygen carriers based on Ni, Fe and Cu. They used SCM for plate-like geometry for a Cu-based oxygen carrier prepared by

impregnation and spherical grains geometry for freeze-granulated Ni and Fe-based oxygen carriers for the interpretation of the results. The authors concluded that both reduction and oxidation reactions are controlled by chemical reaction resistance [80, 87, 104]. Only in the case of NiO reduction with H_2 was diffusion resistance included in the model [104]. The value of the activation energy for the reduction reaction was dependent on the fuel gas used and varied between 14 and 78 kJ/mol; the activation energy for oxidation reaction was between 7 and 15 kJ/mol. The reaction order found was in the range of 0.25 and 1 depending on the reaction gas and oxygen carrier. Son and Kim investigated the kinetics of NiO-Fe_2O_3/bentonite particles using methane as fuel and found that the modified volumetric model is the best representation of the reduction reaction, whereas the SCM is the best representation of oxidation reaction [105]. The values of activation energy found were in the range of 30-60 kJ/mol and 2-6 kJ/mol for reduction and oxidation reaction respectively, depending on the NiO/Fe_2O_3 ratio in the particles. Readman et al. investigated the kinetics of NiO/$NiAl_2O_4$ and found a two-step reduction behaviour [106]. First, reduction reaction is very fast where oxygen transport to the particle surface is not rate-limiting. This is followed by slower reduction where oxygen transport through the particle becomes a rate-limiting step. The reaction order with respect to H_2 and O_2 found was 1, whereas the reaction order with respect to CH_4 was slightly less than 1.

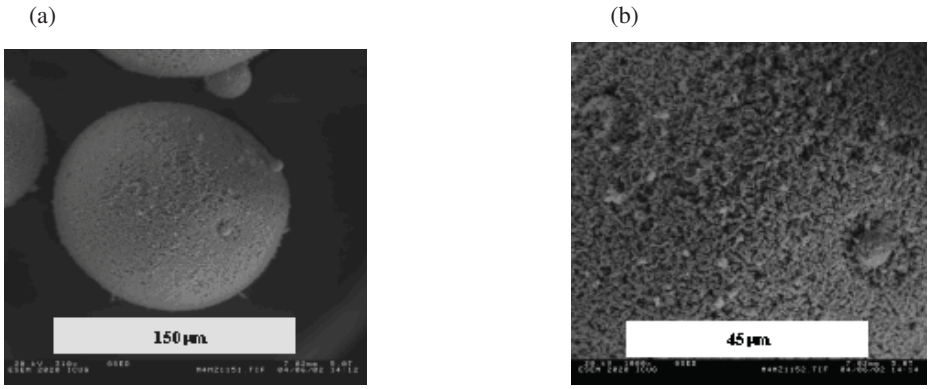

Figure 10: ESEM image of Mn_3O_4/Mg-ZrO_2 sintered at 1150 °C.

The kinetic of two promising types of freeze-granulated particles was investigated in this work; NiO/$MgAl_2O_4$ and Mn_3O_4/Mg-ZrO_2 (paper III & IV). During the preparation of the particles, small primary particles of MeO and inert support of less than 10 µm in size are physically mixed and prepared into slurry that can easily be atomized into drops of larger size. Thus, the particles are composed of relatively large individual grains/primary particles and as a consequence, the particles have rather high porosity. This was also confirmed by ESEM images of the surface of the particles (Figure 10). It can therefore be assumed that the particles are composed of spherical grains, which react with the same reaction rate throughout the particle following the SCM.

During the reaction of MeO with methane several resistances can affect the rate of reaction. The reaction could be controlled by external mass transfer, gas diffusion into the particle pores, diffusion into the solid product layer or the chemical reaction. The mass transfer resistance was reduced as much as possible by working with high gas flow and a small mass sample in the TGA experiments. The effect of particle size was investigated with particles in the size range 90-250 µm and no effect on reaction rate was observed. This observation

suggests that internal diffusion resistance is not limiting the rate of reaction. The oxygen carrier particles are porous and porosity increases as e.g. NiO is reduced to Ni because of the difference in molar density of NiO and Ni. Garcia-Labiano et al. showed that for the experimental conditions (porosity, type and content of MeO, particle size, reaction rate) similar to those used in this work, internal diffusion resistance is not important and the reaction takes place inside the whole particle at the same time [88]. Moreover, the temperature changes inside the particle that are due to reactions were not important and the particles could be considered isothermal. Chemical reaction seems to be the only resistance that is controlling the reduction reaction rate of these types of oxygen carriers with methane.

For the kinetic determination of the $NiO/MgAl_2O_4$ particles a SCM with chemical reaction control was used (Paper III), whereas for the $Mn_3O_4/Mg\text{-}ZrO_2$ particles a SCM was initially used to predict the results. However, model results do not fit quite well with the experimental results. Therefore for kinetic determination it was assumed that that the conversion follows a linear dependence with the reacting time. It was speculated that oxygen from the grain diffuses to the surface of the grain and reacts with methane, as was suggested in Readman et al [106]. Here, the linear model was also chosen because of the form of conversion-time curves obtained experimentally. Readman et al. [106] used the same model to interpret the results in which spherical particles were produced by dissolution method. The kinetic equation for the linear model is

$$\frac{t}{\tau_i} = X_i \tag{23}$$

and

$$\frac{1}{\tau_i} = \frac{\mathrm{d}X_i}{\mathrm{d}t} \tag{24}$$

where τ is the time for complete conversion of the particle and calculated from

$$\tau_i = \frac{1}{k_i^* C_g^n} \tag{25}$$

where k^* is a kinetic constant. Therefore, equation 21 can be rewritten as

$$\ln\left[\frac{\mathrm{d}X_i}{\mathrm{d}t}\right] = \ln\left(k_i^*\right) + n \ln C_g \tag{26}$$

Assuming that the kinetic constant follows an Arrhenius type of expression, it can be obtained at different temperatures from the expression

$$k_i^* = k_{0,i}^* \cdot e^{E_i / RT} \tag{27}$$

7. Results

This thesis consists of four papers. The work was started by investigating some metal oxide prepared by impregnation on SiO_2 support, which had never previously been investigated as a support before for oxygen carrier particles at that time. The particles were tested in a laboratory batch fluidized bed reactor and the focus was to evaluate the oxygen carriers with respect to CLR. All metal oxides showed interaction with SiO_2 at higher temperatures and a decrease in reactivity as a function of cycle was observed. This decrease was due to the reaction between inert support and active MeO. However, NiO showed a high selectivity towards hydrogen formation and was identified promising for CLR (paper I). In paper II, the reactivity of eight different oxygen carriers was examined in a TGA using methane and air alternatingly. The four particles based on SiO_2 were tested, in addition to oxides of Fe, Ni, Mn and Cu on $MgAl_2O_4$. In the fluidized bed experiments during the oxidation period it was not possible to get a rate that is not limited by the supply of oxygen. This is because all the oxygen entering the reactor is reacting with the oxygen carrier. This problem was solved by performing tests in TGA, where the particles are exposed to a well defined reactant gas concentration. $NiO/MgAl_2O_4$ showed a promising reactivity both during reduction and oxidation (paper II) and should be a suitable oxygen carrier both for CLC and CLR. Because at a high degree of solid conversion CO_2 and water are formed, which are the desired products in CLC: at low degree of conversion selectivity is mostly towards hydrogen, which is desired in CLR.

In previous studies, $NiO/MgAl_2O_4$ and Mn_3O_4/Mg-ZrO_2 prepared by freeze granulation were investigated in batch and continuous laboratory fluidized-bed reactors and showed very promising results. $NiO/MgAl_2O_4$ showed a promising reactivity both for both CLC and CLR, whereas Mn_3O_4/Mg-ZrO_2 showed an excellent reactivity for CLC [24-27, 64, 67]. However no kinetic data were available for these promising oxygen carriers. Thus a detailed kinetic investigation of $NiO/MgAl_2O_4$ and Mn_3O_4/Mg-ZrO_2 was done using methane and air in a TGA (paper III and paper IV). Knowledge of the kinetic data has a great importance in the design of a CLC system, because it is related with the solid inventory necessary in the fuel and air reactors to transfer the oxygen demanded by the combustion of the fuel gas. Below some important results are presented from these investigations, while the details of the investigation can be found in the papers in the appendix.

7.1 Investigation of SiO_2 supported oxygen carriers in fluidized bed

Figure 11 shows the outlet gas concentration from the fluidized bed reactor during a reduction period using particles of NiO and CuO supported on SiO_2. For CuO/SiO_2 (Figure 11a), initially incoming reacts with oxygen present in the particles to form CO_2 and water. However as the oxygen in the particles is reduced, unconverted methane is released, as was the case of Fe_2O_3/SiO_2 (Figure 6).
In case of NiO/SiO_2 initially incoming methane is oxidized to CO_2 and water when a higher amount of oxygen is available in the particles. However, as oxygen in the particles is depleted, methane reforming or pyrolysis starts on metallic Ni sites on the particles and a large amount of hydrogen is produced (Figure 11 b) Thus, these particles may be suitable for both CLC and CLR, although the applicable conversion levels are different.

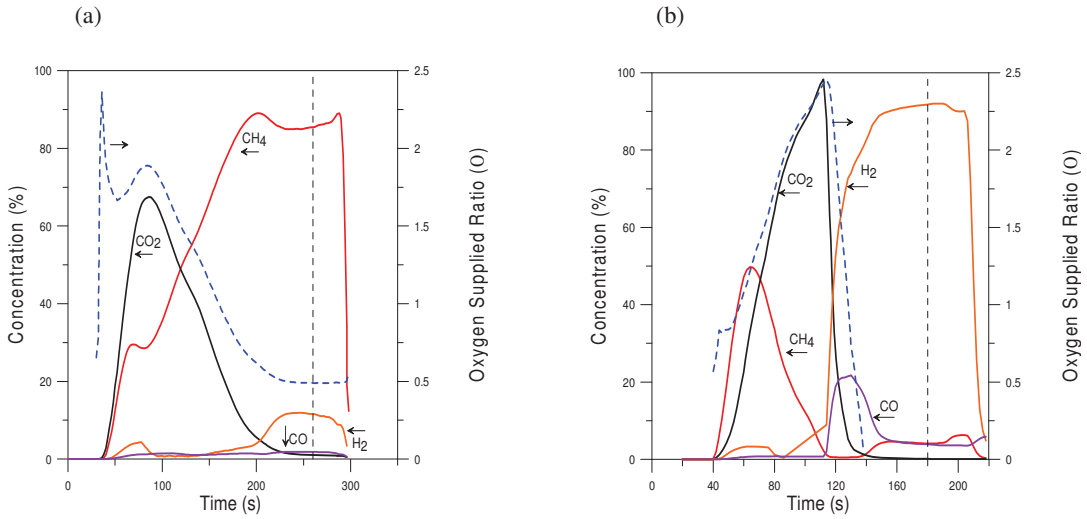

Figure 11 Outlet gas concentrations from the fluidized-bed reactor for the reactivity experiment with (a) CuO/SiO_2 (2^{nd} reduction period) and (b) NiO/SiO_2 (4^{th} reduction period) at 800 °C. The vertical dashed line indicates the switch to inert atmosphere.

7.1.1 Reactivity during reduction and oxidation

Particles of NiO, CuO, Mn_2O_3 and Fe_2O_3 supported on SiO_2 were investigated in the fluidized- bed reactor. Figure 12a shows the rate of mass conversion, dω/dt, as a function of mass conversion ω, for the 5^{th} reduction period. All oxygen carriers were tested at 950°C, while CuO/SiO_2 and NiO/SiO_2 were also tested at 800°C. To facilitate the comparison between all the oxygen carriers, it was assumed that the sample had ω=1 i.e. fully oxidized prior to the reduction periods. It can be seen in the Figure 12a that NiO/SiO_2 and CuO/SiO_2 are the most reactive and Fe_2O_3/SiO_2 is the least reactive under reducing conditions. With the exception of CuO all the metal oxide had a rather low extent of reaction. The reason may be the formation of metal silicate at high temperatures, which may not react with CH_4 and in case of NiO also the agglomeration of active phase on the support.

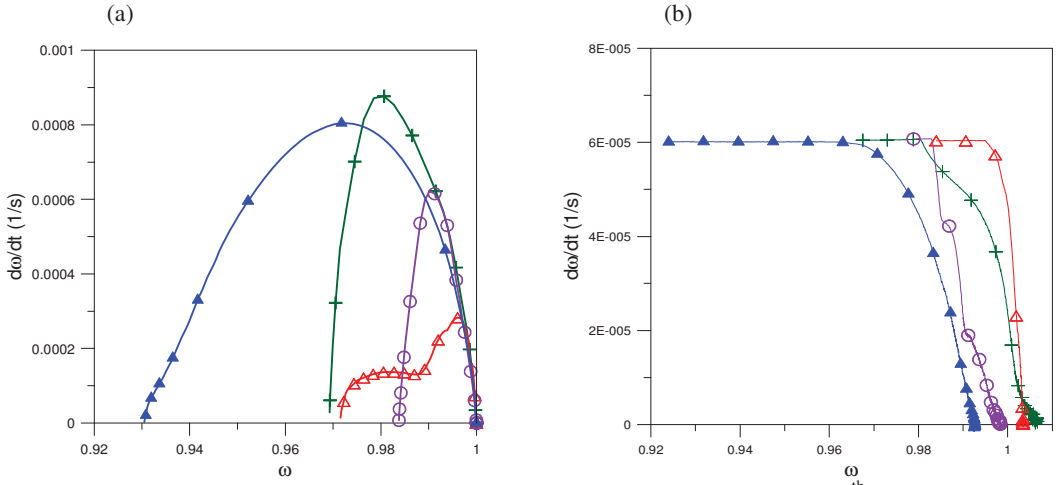

Figure 12 Rate of mass conversion (dω/dt) as a function mass conversion (ω) for the (a) 5^{th} reduction period and (b) 5^{th} oxidation period at 950 °C for SiO_2 supported NiO (+), Mn_2O_3 (○), Fe_2O_3 (Δ) and CuO (▲) at 800°C.

As can be seen from Figure 11, when oxygen supplied ratio is 1, the CuO has considerable amounts of CH_4 at the outlet of the reactor, while NiO has no methane and substantial amounts of hydrogen produced. During oxidation, the rate is constant in the beginning of the period; (Figure 12b), which means that all the oxygen entering the reactor is reacting with the oxygen carrier. Thus, a comparison of rates, which are not limited by the supply of oxygen, is not possible with this experimental method. CuO has the highest and Mn_2O_3 has the lowest extent of reaction during oxidizing conditions. Both NiO and Mn_2O_3 particles could not be oxidized back to the initial condition at 950°C.

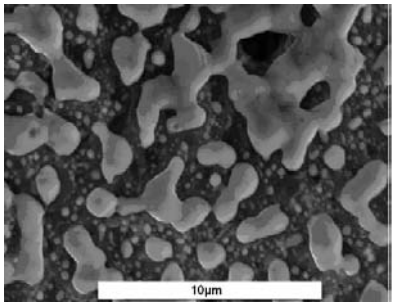

Figure 13: SEM image of reduced NiO/SiO_2 at 950°C.

The reason may be the formation of irreversible manganese silicate in case of Mn_2O_3/ SiO_2, which was seen in the XRD analysis of the reacted sample and for NiO agglomeration of active phase on the support (Figure 13) and possibly silicate formation. Oxidation of reduced iron oxide was very fast and particles were fully oxidized in 400 s (Figure 6b).

7.1.2 Effect of temperature

NiO/SiO_2 showed a higher selectivity towards H_2 formation in comparison to the other oxygen carriers; however the extent of the reaction decreased as a function of cycle for NiO at 950°C. Thus it was investigated at different temperatures, i.e. at 850 and 800°C, to determine if the deactivation could be avoided. A reactivity comparison is shown in Figure 14 for reduction and oxidation at different temperatures for NiO/SiO_2.

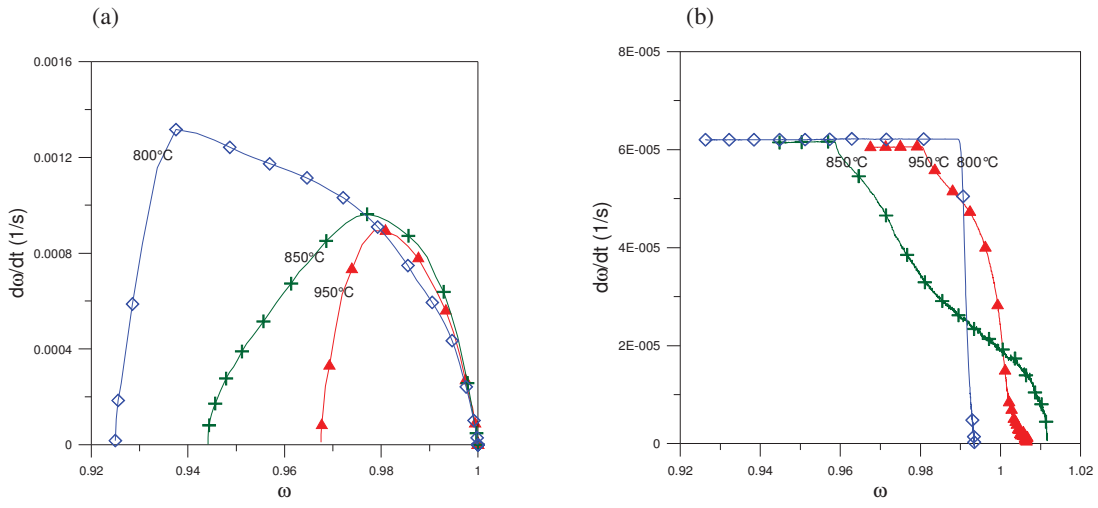

Figure 14 Reactivity comparison for (a) 4th reduction and (b) 5th oxidation periods at 800 (◊), 850 (+) and 950°C (▲) for NiO/SiO_2

As shown in the Figure 14a, NiO has the highest reaction rate and the extent of reaction at 800 °C. The oxygen ratio is 0.074 for this carrier. If all of the NiO had converted to Ni the $\Delta\omega$ would be equal to R_o. This was achieved in the experiment conducted at 800°C. The oxidation rate was also improved at a lower temperature (Figure 14b). The reactivity is much higher at 800°C as compared with 850 and 950°C at higher degrees of ω. NiO/SiO_2 particles produced by freeze granulation did not show deactivation even at high temperature see appendix.

7.1.3 Effect of cycle number

A clear decrease in reactivity was seen at 950 °C for NiO/SiO_2, Fe_2O_3/SiO_2 and Mn_2O_3/SiO_2, which is likely due to the formation of irreversible silicate of Mn and Fe, which were found in the XRD analysis of the reduced sample (Table 5) and agglomeration, and possibly also silicate formation for NiO/SiO_2 (Figure 13).

Table 5 *XRD results for fresh and reduced particles from fluidize- bed reactor experiments*

Oxygen carrier	Fresh sample	Reduced sample
Fe_2O_3/SiO_2	Fe_2O_3, SiO_2	Fe_3O_4, Fe_2SiO_4, FeO^*, SiO_2
NiO/SiO_2	NiO, SiO_2	Ni, SiO_2
Mn_2O_3/SiO_2	Mn_2O_3, MnO_2^*, $Mn_5O_8^*$, SiO_2	Mn_2SiO_4, Mn_3O_4, MnO^*, $MnSiO_3^*$, SiO_2
CuO/SiO_2	CuO, Cu_2O^*, SiO_2	Cu, Cu_2O^*, SiO_2

*minor phase

7.1.4 Carbon deposition

By the release of CO_2 and CO during the inert period or in the beginning of the oxidation period, it was possible to establish if there was carbon formation on the particles under the reducing period in the fluidized-bed experiment. A small amount of carbon was formed on Mn_2O_3/SiO_2 and CuO/SiO_2 particles at 950 and 900°C respectively. A small CO_2 peak in the beginning of oxidation (Figure15) showed that carbon was formed on Mn_2O_3/SiO_2 particles.

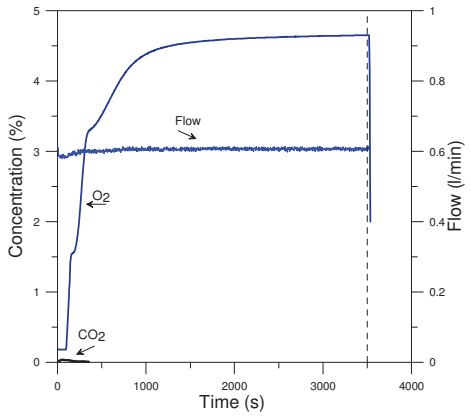

Figure 15 Outlet gas concentration from the fluidized-bed reactor during the 3rd oxidation period in the reactivity experiment with Mn_2O_3/SiO_2. The vertical dashed line indicates the switch to inert atmosphere.

A similar type of behavior was seen for CuO. Carbon was deposited on NiO/SiO_2 particles in the experiments conducted at all three temperatures i.e. at 950, 850 and 800°C. In contrast to the results for the Mn and Cu carriers, there was oxidation of this deposited carbon both during the inert and oxidizing periods. Because no oxygen was added in the gas phase during the inert period; CO may be formed through a solid-solid state reaction between the deposited carbon and the oxygen present in the reduced particle. Thus, there is a clear difference in the carbon oxidation mechanism between the particles. For the manganese and copper based particles, the deposited carbon on the reduced samples did not react with lattice oxygen during the inert period, but was oxidized first when gas-phase oxygen was added to the reactor.

7.1.5 Selectivity towards H_2 formation

In comparison with CLC, full conversion of natural gas to CO_2 and H_2O is not a goal in CLR, but instead a maximized H_2 production is desired. All the oxygen carriers except NiO/SiO_2 showed poor selectivity towards H_2 formation. In case of CuO/SiO_2, Fe_2O_3/SiO_2 and Mn_2O_3/SiO_2, generally the incoming methane reacts with the oxygen present in the particles to form to CO_2 (and H_2O). However, as the oxygen content decreases in the particles, there was some formation of CO and H_2 with the release of unconverted CH_4 (Figure 11a).

NiO/SiO_2 showed high selectivity toward H_2 formation at all temperatures. Initially CH_4 reacts very fast with the particles to form CO_2, but as the oxygen content decreases in particles, CH_4 reforming or pyrolysis starts in the presence of metallic Ni and a large amount of H_2 is formed (Figure 11b). The amounts of H_2 produced with CuO/SiO_2 and NiO/SiO_2 carriers can be compared (Figure 11). It is clear that NiO/SiO_2 produces a large amount of H_2 compared with CuO/SiO_2.

7.2 Investigation of $MgAl_2O_4$ and SiO_2 supported oxygen carriers in TGA

Particles of NiO, CuO, Fe_2O_3 and Mn_2O_3 supported on SiO_2 and $MgAl_2O_4$ were tested at 800-1000 °C in a TGA. As explained earlier, the TGA is a good tool for evaluation of reactivity of oxygen carrier particles. However, as it was not possible to measure the product gases, the applicability towards CLR is limited. A gas mixture of 10% CH_4, 10% H_2O and 5% CO_2 in nitrogen was used for reduction and 5% O_2 in nitrogen for oxidation. The concentrations were chosen to approximate the average gas concentration to which oxygen carrier should be exposed to in the fuel and air reactors. The SiO_2-based carriers are the same as those tested in the fluidized-bed reactor. In most of the experiments mass was not stable prior to the first reduction period. Thus, 2nd reduction cycle was used as the reference cycle. It was also found that either first reduction was slower or faster depending on the oxygen carrier used in the experiment. This behavior may be due to internal restructuring of the fresh oxygen carrier during the first cycle.

7.2.1 Conversion

Figure 16 shows the conversion, X, as a function of time for the 2nd reduction and 3rd oxidation period for both SiO_2 (Figure 16a) and $MgAl_2O_4$ (Figure 16b) supported oxygen carriers. The reduction and oxidation of NiO, Fe_2O_3 and Mn_2O_3 carriers were performed at

950°C, whereas CuO carriers were tested at 800°C. SiO_2 supported NiO and CuO reduced to a value of X equal to 0 and 0.10, see Figure 16a, whereas $MgAl_2O_4$ supported NiO and CuO reduced to a value of an X equal to 0.19 and 0.07 respectively (Figure 16b). The reason for the lower degree of reduction of $MgAl_2O_4$ supported NiO may be the presence of nickel aluminates in the fresh sample, which are formed during the sintering of the oxygen carrier. This was confirmed by X-ray diffraction (Table 6) and means that a lower fraction of oxygen is available for the reaction. Fe_2O_3 and Mn_2O_3 on SiO_2 were reduced to an X value of 0.6 and 0.17, respectively (Figure 16a), whereas Fe_2O_3 and Mn_2O_3 on $MgAl_2O_4$ were reduced to an X value of 0.7 and 0.22, respectively (Figure 16b). The reducing gas mixture used should be able to reduce the iron oxide all the way to Fe thermodynamically. Thus, it is likely that the reaction is hindered by kinetic effects, i.e. the reaction rate is controlled by product layer diffusion.

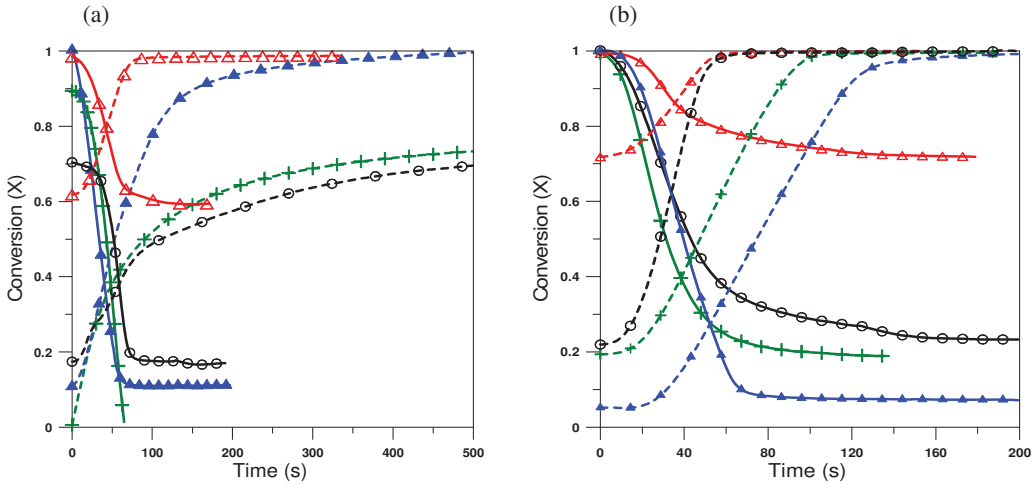

Figure 16 Conversion as a function of time for 2nd reduction period (solid line) and 3rd oxidation period (dashed line) for (a) SiO_2 and (b) $MgAl_2O_4$-supported NiO (+), Mn_2O_3 (○), Fe_2O_3 (Δ) at 950 °C and CuO (▲) at 800°C in a TGA.

During oxidation, Fe_2O_3 and CuO supported on SiO_2 were almost fully oxidized to an X value equal to 1. However, NiO and Mn_2O_3 could only oxidize to an X value equal to 0.75. The reason for the lower X value for oxidation may be the formation of irreversible silicates of Mn as a result of a reaction between active phase and inert support and agglomeration on the support for Ni. This observation is similar to the results seen during the fluidized bed experiments. All $MgAl_2O_4$-supported oxygen carriers were fully oxidized within 200 s during oxidation (Figure 16b).

Table 6 Phases identified with *X-ray powder diffraction*

Oxygen carrier	Fresh sample
NiO/ $MgAl_2O_4$	NiO, $NiAl_2O_4$, $MgNiO_2$, $MgAl_2O_4$
Mn_2O_3/ $MgAl_2O_4$	$MnAl_2O_4$, $MgAl_2O_4$
CuO/ $MgAl_2O_4$	CuO, $CuAl_2O_4$, $MgAl_2O_4$
Fe_2O_3/ $MgAl_2O_4$	Fe_2O_3,$MgAl_2O_4$, Fe_3O_4,

7.2.2 Reduction rate

Figures 17a and 17b show the rate of mass conversion, dω/dt, as a function of mass conversion, ω, for the 2nd reduction period of SiO_2 and $MgAl_2O_4$-supported oxygen carriers respectively. It can be seen that both NiO and CuO supported on SiO_2 and $MgAl_2O_4$ had high reaction rate and a high extent of reaction during the reduction. However, the extent of reaction is low for NiO/$MgAl_2O_4$, where Δω=0.062, which can be compared with NiO/SiO_2, where Δω=0.072. The reason for the lower extent of reaction for $MgAl_2O_4$-supported NiO is the presence of nickel aluminates in the fresh sample, which are not reducible or reduce at a slow rate. Fe_2O_3 and Mn_2O_3 on both SiO_2 and $MgAl_2O_4$ supports showed a lower reaction rate and a lower extent of reaction. The reason for the lower extent of reaction of Mn_2O_3/SiO_2 may be the formation of irreversible manganese silicates during the reaction with CH_4 and for Fe_2O_3/SiO_2 the reaction may be hindered by kinetic effects as explained previously. In the case of $Mn_2O_3/MgAl_2O_4$, a large amount of manganese aluminates was present in the fresh sample, which may be the reason for the lower extent of reaction (Table 6).

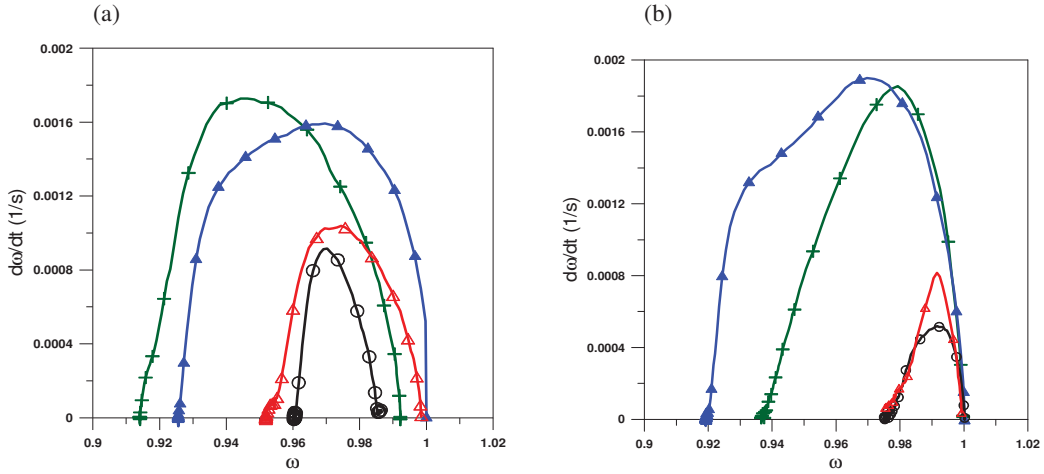

Figure 17 Rate of mass conversion (dω/dt) as a function mass conversion (ω) for the 2nd reduction period (a) SiO_2- and (b) $MgAl_2O_4$-supported NiO (+), Mn_2O_3 (○), Fe_2O_3 (Δ) at 950°C and CuO (▲) at 800°C.

7.2.3 Oxidation rate

With the exception of Mn_2O_3, all SiO_2-supported oxygen carriers initially showed a similar rate of oxidation with the rate slowing down the degree of oxidation increased. The highest rates correspond to 4-5 %/min on the mass basis for SiO_2 oxygen carriers (Figure 18a).
In the fluidized-bed reactor, the obtained oxidation rate was limited by the supply of oxygen. However, in TGA it was possible to obtain a reaction rate at a certain mass conversion, where the oxygen concentration was well defined. For CuO, the oxidation rate starts to drop to approximately ω= 0.95 but stabilizes at ω = 0.96 and then gradually decrease to zero (Figure 18a). This behaviour is most probably because Cu is oxidized to Cu_2O in the beginning of the oxidation period and Cu_2O starts to oxidize to CuO at approximately ω = 0.96. Mn_2O_3/SiO_2 oxidized at a very slow reaction rate. Further, it can be observed in Figure 18a that initially the reaction rate reaches a maximum then decreases, and again increases for a while and subsequently slows down to zero at the end. The same behaviour for Mn_2O_3/SiO_2 was seen in fluidized-bed experiment. This is similar to the experiment with copper and may also be due

to the initial oxidation of MnO to Mn_3O_4 followed by the reaction of Mn_3O_4 to Mn_2O_3. The oxidation behaviour of the $MgAl_2O_4$ based carriers was considerably different compared with the SiO_2-based carriers. The $MgAl_2O_4$ particles are oxidized back to the fully oxidized state after oxidation (Figure 17b).

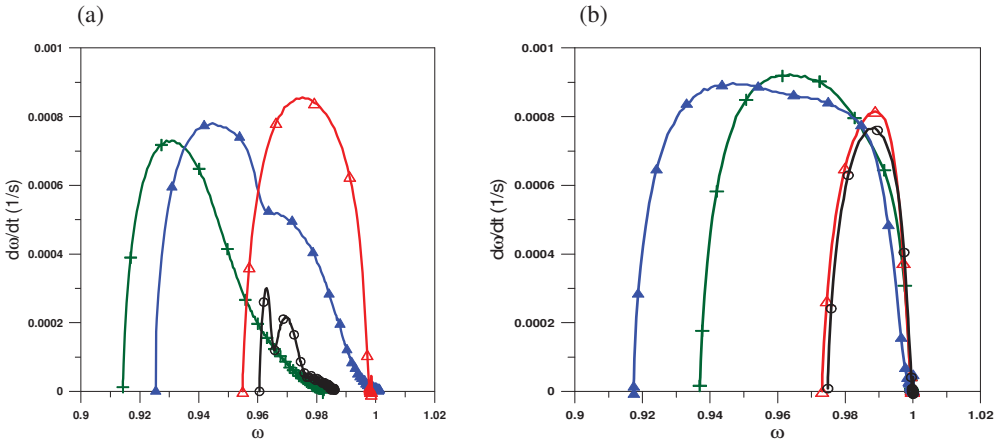

Figure 18 Rate of mass conversion (dω/dt) as a function mass conversion (ω) for the 3rd oxidation period (a) SiO_2- and (b) $MgAl_2O_4$-supported NiO (+), Mn_2O_3 (○), Fe_2O_3 (Δ)at 950°C and CuO (▲) at 800°C.

Further, the initial oxidation rate was similar for all oxygen carriers, (Figure 18b). The maximum rates were similar as with the SiO_2-based particles, except Mn_2O_3/SiO_2, i.e. approximately 4-5%/min on a mass basis. However, in contrast to SiO_2-based carriers, all of the $MgAl_2O_4$-based carriers were fully oxidized back to the initial degree of conversion.

7.2.4 Effect of cycle number

As observed in the fluidized-bed experiments, all SiO_2-supported carriers showed a similar type of behaviour as a function of cycle number. All of the $MgAl_2O_4$-supported oxygen carriers showed a relatively constant reaction rate during reduction and oxidation as a function of number of cycle, i.e. little or no deactivation. However, a small increase in the reactivity was observed with $CuO/MgAl_2O_4$ and $NiO/MgAl_2O_4$ as a function of number of cycle. This was probably due to the change in structure of the particles during the redox experiments.

7.2.5 Effect of temperature

$NiO/MgAl_2O_4$ showed a promising reactivity during reduction and oxidation. Thus this oxygen carrier was also tested at different temperatures, 800, 850 and 1000°C in the TGA in addition to 950°C. During the reducing atmosphere, the highest reactivity was found at 950°C and lowest reactivity at 800°C (Figure 19). The reactivity was lower at 1000 °C than the reactivity at 950°C during the reduction. There were visible structural changes during the reaction at 1000°C (Figure 20b), which may be the cause for lower reactivity.
The oxidation rate was quite high during oxidation at all temperatures but at 1000 °C the rate was highest, reaching a value of almost 0.001 s^{-1} or 6%/min on mass basis (Figure 19b).

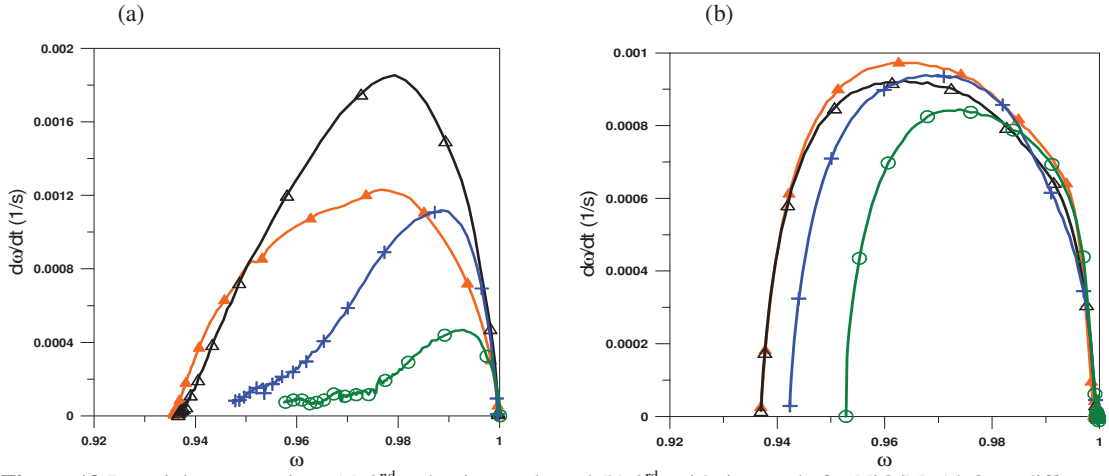

Figure 19 Reactivity comparison (a) 2nd reduction cycle and (b) 3rd oxidation cycle for $NiO/MgAl_2O_4$ at different temperatures 1000°C (▲) 950°C (Δ), 850°C (+) and 800°C (○).

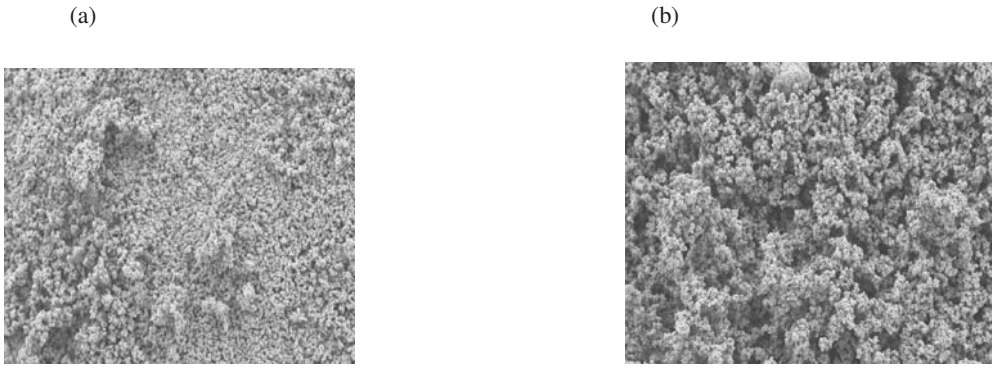

Figure 20. Reduced $NiO/MgAl_2O_4$ at (a) 950°C and (b) 1000°C

7.3 Reduction and oxidation kinetics for $NiO/MgAl_2O_4$ oxygen carrier

$NiO/MgAl_2O_4$ showed excellent reactivity for reduction and oxidation in a TGA experiments (paper II). Later $NiO/MgAl_2O_4$ prepared by freeze granulation was investigated in batch and continuous laboratory fluidized-bed reactors both for CLC and CLR and showed excellent results [25-27, 67]. Thus these type of particles were chosen for a detailed kinetic study. This type of information is important for the design of the reactor system.
The particles were composed of 60 wt% NiO and 40 wt% $MgAl_2O_4$ (Table 3). Some of the NiO reacted inert support and thus reducing the active NiO to 50 wt%. During the preparation of the particle, small primary particles of NiO and $MgAl_2O_4$ of less than 10 µm in size are physically mixed and prepared into slurry that can easily be atomized into drops of larger size. Thus, the particles are composed of relatively large individual grains/primary particles. This was also confirmed by ESEM images of the surface of the particles. Thus, for kinetic determination it was assumed that the particles are composed of spherical grains that react with the same reaction rate throughout the particle following the SCM.

7.3.1 Reduction reaction

In the fuel reactor the oxygen carrier is exposed to different fuel gas concentrations and environments at different locations. At the bottom of the fluidized bed, the oxygen carrier will be in contact with pure fuel while the gas phase will mostly consist of CO_2 and H_2O at the top of the bed. To see the effect of methane concentration and temperature on the reduction of the $NiO/MgAl_2O_4$ carrier, experiments were performed with 5, 10, 15 and 20% CH_4 at different temperatures varying from 800-1000°C. Fuel gas was saturated with water vapours (20%) in all the experiments to avoid carbon formation on the particles. Because steam is produced during the reduction, the presence of H_2O better simulates the conditions in the fuel reactor.

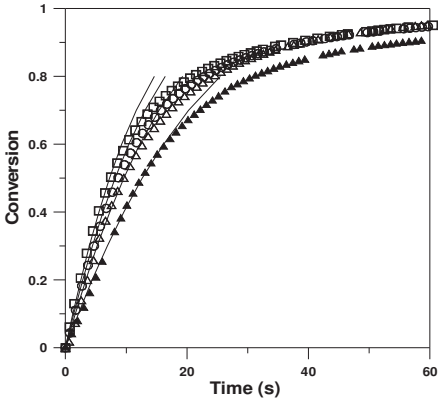

Figure 21: The conversion as a function of time for different CH_4 concentrations for the experiments conducted at 950°C. CH_4 concentrations are 5% (▲), 10 %(Δ), 15% (○) and 20% (□). Continuous line: results predicted by the model using kinetic parameters obtained in this work.

Figure 21 shows the solid conversion as a function of time for the $NiO/MgAl_2O_4$ oxygen carrier with different CH_4 concentrations at 950°C for the 4th reduction period. Initially, the reaction rate is very fast for all experiments; moreover the reaction rate increased with increasing CH_4 concentration. For all concentrations, less than 20 s is needed to obtain a $\Delta X=0.6$.

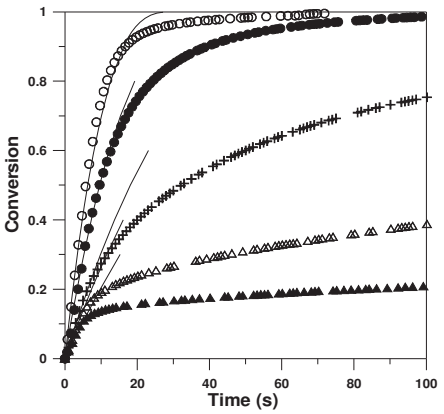

Figure 22: Effect of temperature on the reduction reaction of $NiO/MgAl_2O_4$ with CH_4 (10%) at 800°C (▲), 850°C (Δ), 900°C (+), 950°C (●) and 1000°C (○).Continuous line: results predicted by model using kinetic parameters obtained in this work.

Figure 22 shows the conversion as a function of time obtained with 10% CH_4 concentration at different temperatures. The reaction rate is a function of temperature. The change in conversion was very low at lower temperatures i.e. conversion was only $\Delta X=0.2$ and 0.4 at 800 and 850°C, respectively. It is likely that at the lower temperature the reaction is controlled by two kinds of different resistances; at low solid conversion the reaction rate is likely controlled by chemical reaction and at higher solid conversion (from 0.1 to 1 depending on the temperature) the reaction rate could be controlled by the diffusion in the solid product layer. Because of the slow reduction reaction at lower temperatures, the investigated particles should likely be used at temperatures of 900 °C and above. Here the reaction is controlled by chemical reaction for a substantial part of the conversion interval (Figure 22).

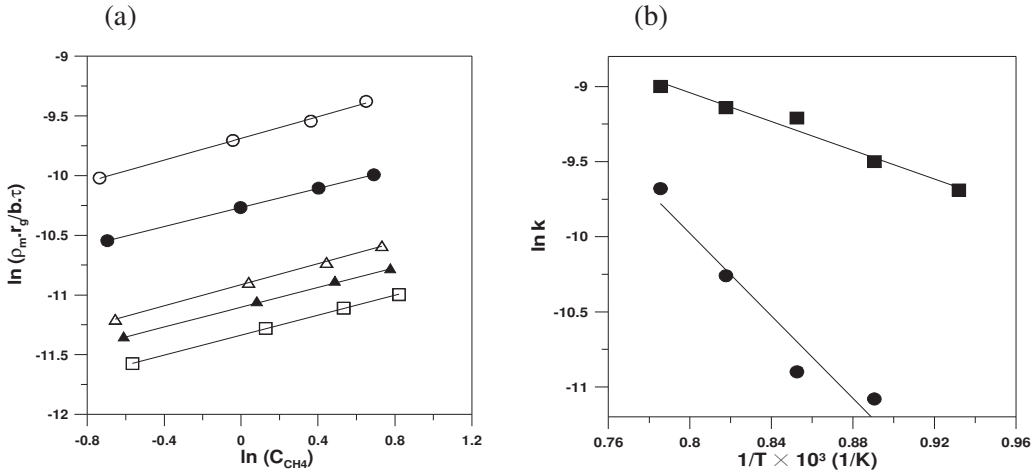

Figure 23: (a) $\ln(\rho_m r_g/b\tau)$ as function of $\ln(C_{CH4})$ to obtain the order of reaction for reduction and the value of k at different temperatures 800°C (□), 850°C (▲), 900°C (Δ) 950°C (●) and 1000°C (○). (b) Arrhenius plot of the reduction and oxidation reaction with the $NiO/MgAl_2O_4$ oxygen carrier. CH_4 (●), O_2 (■).

Figure 23a shows a plot of $\ln(\rho_m r_g/b\tau)$ as a function of $\ln(C_{CH4})$ for the experiments conducted at different temperatures. The slope of the plot was about 0.4 with all temperature, which is the order of reaction n with respect to CH_4. Figure 23b shows the plot used to obtain the values of the kinetic parameters assuming Arrhenius dependence of the kinetic constant with the temperature. The value of activation energy for reduction reaction was found to be 114 kJ/mol while the frequency factor, k_o, was 2.75 $mol^{0.6}m^{-0.8}s^{-1}$. The activation energy obtained here is rather high in comparison with those found for previously investigated Ni-based oxygen carriers. This may due to the addition of Mg in the oxygen carrier, which increases the activation energy for both reduction and oxidation reaction.

The kinetic constant, k, obtained using the frequency factor and activation energy and the order of reaction, n, were used in the SCM equation. The model results are shown together with the experimental data in Figures 21 and 22. The experimental results are represented by symbols and model prediction with continuous lines. It can be seen in Figures 21 and 22 that experimental results obtained at temperature of practical interest (950 and 1000 °C) fit with the prediction model until almost 70 % conversion of the oxygen carrier during reduction. It is unlikely that $NiO/MgAl_2O_4$ will be reduced to such a lower degree of conversion in a real CLC system.

7.3.2 Oxidation reaction

The reduced oxygen carrier from the fuel reactor will be transferred to the air reactor of a CLC system for regeneration. In the air reactor the $NiO/MgAl_2O_4$ oxygen carrier in reduced state will be exposed to different oxygen concentrations varying from 21 % O_2 at the inlet of the reactor and perhaps 4%O_2 at the outlet if 20% of excess air is used in the reaction. To see the effect of oxygen concentrations and temperature several experiments were conducted with different oxygen concentrations between 3 and 15% at different temperatures 800-1000°C.

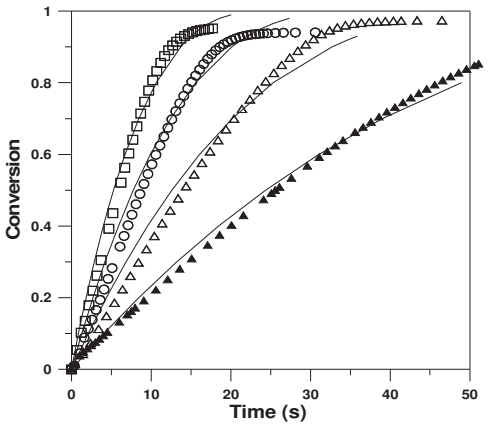

Figure 24: The conversion as a function of time for different O_2 concentrations for the experiments conducted at 1000°C. O_2 concentrations are 3% (▲), 6% (Δ), 10% (○) and 15% (□). Continuous line: results predicted by the model using kinetic parameters obtained in this work.

Figure 24 shows the conversion as a function of time obtained at 1000 °C with different oxygen concentrations for the 4th oxidation period. Also shown are the model calculations using kinetic data obtained below. Clearly, also the oxidation reaction is also very fast and the rate of reaction is a function of oxygen concentration with the higher rates for the experiments with the higher oxygen concentration.

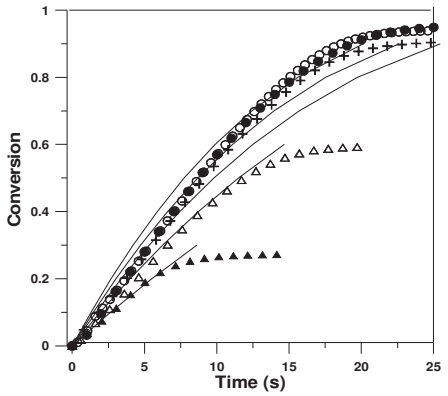

Figure 25: Effect of temperature on the oxidation reaction of $NiO/MgAl_2O_4$ with O_2 (10%) at 800°C (▲), 850°C (Δ), 900°C (+), 950°C (●) and 1000°C (○). Continuous line: results predicted by model using kinetic parameters obtained in this work.

Figure 25 shows the conversion as a function of time obtained at different temperatures with 10% O_2 concentrations. The oxidation rate was found to be a function of temperature; although for higher temperatures i.e. 900, 950 and 1000 °C, there is only a little difference in reaction rate. The low degree of final conversion at 800 and 850 °C is due to the low conversion reached during the reduction period. But in all cases the sample was oxidized back to a fully oxidized sample. The shrinking-core model for spherical grains was also used to model the oxidation reaction. The kinetic model was developed using chemical reaction being the only resistance controlling the reaction. To determine the order of reaction several experiment were conducted at different temperatures with different O_2 concentration. The reaction order, n, of oxidation reaction was obtained by the slope of the plot of $\ln(\rho_m r_g/b\tau)$ vs. $\ln(C_{O2})$ and was about 1, see Figure 26. The results obtained at 800°C have not been included in this figure due to the much lower conversion obtained in the previous reduction step at this temperature.

Figure 23b shows the Arrhenius plot obtained from the oxidation reaction data. The energy of activation for oxidation reaction obtained from the Arrhenius plot was about 40 kJ/mol and pre- exponential factor k_o found was 5.43×10^{-3} m/s. The results obtained with the shrinking-core model fit reasonably well with the experimental results, see Figures 24 and 25, which confirms that chemical reaction controlled the global reaction rate.

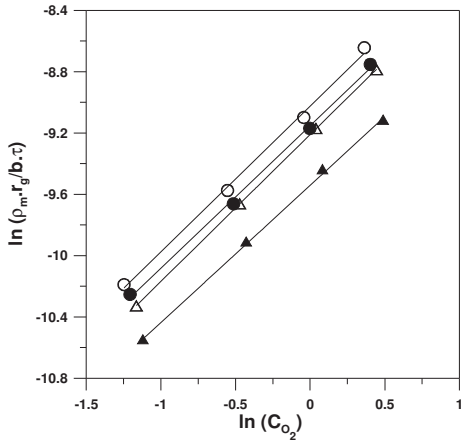

Figure 26: $\ln(\rho_m r_g/b\tau)$ as a function of $\ln(C_{O2})$ to obtain the order of reaction for oxidation and the value k at different temperatures: 850°C (▲), 900°C (Δ) 950°C (●) and 1000°C (○)

7.3.3 Amount of $NiO/MgAl_2O_4$ in the fuel and air reactor

The reactivity data and kinetic parameters obtained were used to estimate the amount of material needed in the air and fuel reactors of a CLC system. It was found that total solid inventory varies with the solid conversion at the inlet of the fuel and air reactor. In the calculations it was assumed that the air reactor was operated at 1000 °C and the fuel reactor at 950°C. This corresponds to a conversion difference of 0.18 between the reactors, and a recirculation rate of 4.15 kg s^{-1} MW_f^{-1}. The minimum solid inventory found was 22 kg/MW_f (Figure 27). The method for calculating the solid inventory has been discussed in detail in paper III.

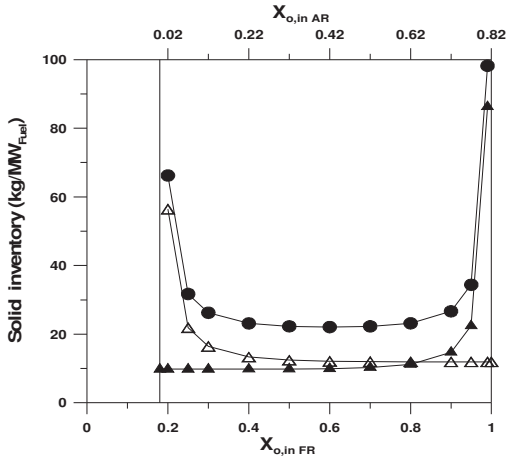

Figure 27: Solid inventory as a function of solid conversion at the inlet of fuel reactor ($X_{o,inFR}$) and air reactor ($X_{o,inAR}$) m_{FR} (Δ),m_{AR} (▲) and m_{total} (●).

7.4 Reduction and oxidation kinetics for the Mn_3O_4/Mg-ZrO_2 oxygen carrier

In general, only a limited work has been performed with manganese based oxygen carriers, which is likely due to the higher interaction of manganese oxide with inert material to form irreversible compounds. The oxygen carrier Mn_3O_4/Mg-ZrO_2 produced by freeze granulation has been investigated in batch and continuous laboratory fluidized-bed reactors. This oxygen carrier has shown excellent results [24, 64] and thus was chosen for detailed kinetic study. The particles were composed of 40% Mn_3O_4 and 60% Mg-ZrO_2 used kinetic investigation. The particles may have different properties compared with pure manganese oxide. It was observed during the experiments that Mn_2O_3 was not formed even at 800 and 850°C. This was later confirmed by the XRD analysis of samples oxidized at 800-950°C. Thus, the difference between m_{ox} and m_{red} in equations (14 and 15) was calculated on the basis of the transformation between Mn_3O_4 and MnO. More details about this can be found in paper IV. For kinetic determination it was assumed that the conversion follows a linear dependence with the reacting time. This model was chosen because of the form of the conversion-time curves obtained experimentally.

7.4.1 Reduction reaction

The oxygen carrier particles will be exposed to different CH_4 concentrations and product gases at different location in the fuel reactor. To see the effect of the product gases on the reduction reaction different experiments were performed by adding 5-20% CO_2 and 10-25% steam with the fuel gas. However, no change in reaction rate was observed indicating that reaction products have no effect on the reduction reaction.

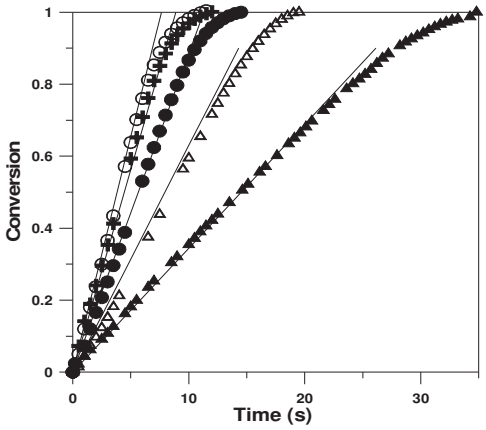

Figure 28: Effect of CH_4 concentration 5% (▲), 10 %(Δ), 15% (•), 20% (+) and 25% (○) on the reduction reaction for Mn_3O_4/Mg-ZrO_2 at 950 °C. Continuous line: results predicted by the model using kinetic parameters obtained in this work.

The effect of methane concentration and temperature on reduction reaction was studied by performing experiments with 5- 25% CH_4 at different temperatures varying from 800-950°C. 20% water vapors were added with reducing gas in order to avoid any carbon formation on the particles and simulate the condition to which the particles will be exposed to in a real CLC conditions. Figure 28 presents the experimental results of different CH_4 concentrations at 950°C. The reaction rate increases by increasing the CH_4 concentration. The experimental curves are almost straight lines. Further, the reaction rate is very fast even at low concentration and the oxygen carrier is completely reduced within 30 s, when the CH_4 concentration is 5%. Figure 29 shows the conversion as a function of time at obtained with a 20% CH_4 concentration at different temperatures. It can be clearly seen that the reaction rate is a function of temperature. The oxygen carrier particles were completely reduced at all temperatures.

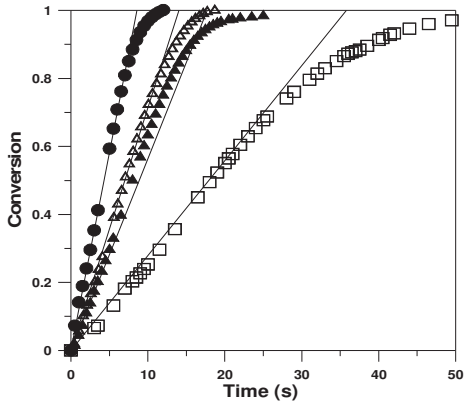

Figure 29: Effect of temperature on the reduction reaction of Mn_3O_4/Mg-ZrO_2 with CH_4 (20%) at 800(□), 850(▲), 900(Δ), 950(●)°C and Continuous line: results predicted by the model using kinetic parameters obtained in this work.

At higher temperatures the reaction rate is very fast and particles are completely reduced within 15 s. At a lower temperature i.e. at 800 °C until X_r=0.8, the reaction rate is very fast and then the reaction rate slows down. It seems as two kinds of resistances are controlling the

rate of reaction at 800°C, first the reaction is controlled by chemical reaction and when most of the particles has reacted, the product layer is formed and oxygen transport through the particle to the surface becomes a rate limiting. However at higher temperatures i.e. above 850 °C the product layer diffusion resistance becomes negligible and reaction is mostly controlled by chemical reaction.

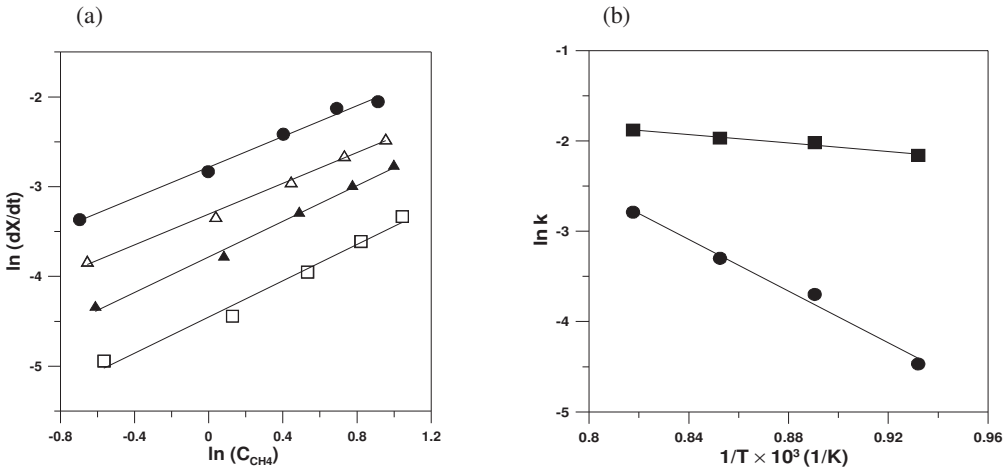

Figure 30: (a) Plot of ln (dX_r/dt) as a function of ln (C_{CH4}) to obtain the order of reaction for reduction and the value k at different temperatures 800(□), 850(▲), 900(Δ) 950(●)°C. (b) Arrhenius plot of the reduction and oxidation reaction with Mn_3O_4/Mg-ZrO_2 oxygen carrier.CH_4 (●), O_2 (■).

In real CLC it is unlikely that the Mn_3O_4/Mg-ZrO_2 oxygen carrier will be reduced to such a high degree of conversion and further, the temperature in the fuel reactor is expected to be well above 800 °C. Thus, it was assumed that chemical reaction is the only resistance controlling the reaction of methane with the oxygen carrier at CLC conditions, and therefore only the parameters corresponding to the resistance were determined in this investigation.

Figure 30a shows ln(dX/dt) as a function of ln(C_{CH4}) for the experiments conducted at different temperatures. The slope of the plot was about 1 at all temperatures, which is the order of reaction with respect to CH_4. Figure 30b shows the plot used in obtaining the values of the kinetic parameters assuming Arrhenius dependence with the temperature for kinetic constant. The value of activation energy obtained for the reduction reaction was 119 kJ/mol and the frequency factor $k^*_{0,r}$ was 7631 $m^3\,mol^{-1}\,s^{-1}$.

The experimental data was fitted using the kinetic parameters obtained; see continuous lines in Figures 28 and 29. The experimental results are represented by the symbols and the model results with the continuous line. It can be seen in Figure 28 and 29 that experimental results obtained at all temperatures fit with the model results for about 90 % of the conversion, with the exception at 800°C, where the experimental results fit with model prediction for about 80% of the conversion. Because of the endothermic nature of the reaction of Mn_3O_4 with CH_4, it is unlikely that oxygen carrier particles will be reduced to such a higher degree of conversion to avoid a major temperature drop in the fuel reactor of a real CLC system. Further, the temperature in the fuel reactor is expected to be well above 800°C. Thus, product layer diffusion resistance was neglected and the only resistance used in developing the prediction model is chemical reaction.

7.4.2 Oxidation reaction

During oxidation at the air reactor, the particle will be in contact with 21% O_2; however, at the top of the bed the oxygen concentration will be about 4% provided that 20% excess air is used in the air reactor. Therefore, it is important to know the variation of the reaction rate with the oxygen concentration, as well as with the temperature.

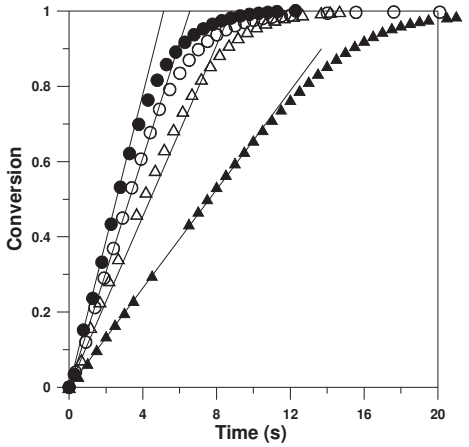

Figure 31: Effect of 3% (▲), 6% (Δ), 10% (○) and 15% (●) O_2 concentration on the oxidation reaction for Mn_3O_4/Mg-ZrO_2 at 950 °C and Continuous line: results predicted by the model using kinetic parameters obtained in this work.

The kinetics of oxidation reaction was investigated by performing experiments using 3-15 % O_2 in nitrogen at different temperatures 800-950°C. Figure 31 shows the conversion as a function of time obtained at 950°C with 3, 6, 10 and 15% oxygen concentration. Oxidation reaction was very fast with all the O_2 concentrations investigated. The reduced oxygen carrier was fully oxidized back to the initial condition within 20 s even when the oxygen concentration was only 3 %. Figure 32 shows conversion as a function of time obtained with 10% O_2. The reaction rate was a function of temperature, however only a little difference in reaction rate was observed at temperatures above 850°C.

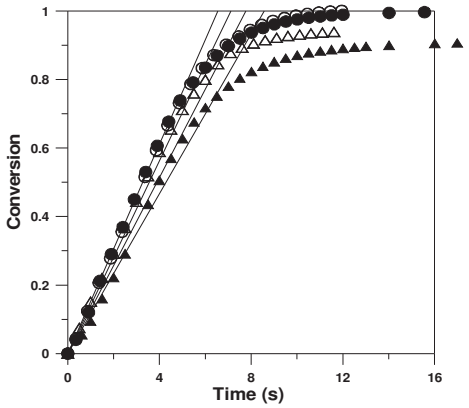

Figure 32: Effect of temperature on the oxidation reaction of Mn_3O_4/Mg-ZrO_2 with O_2 (10%) at 800(▲), 850(Δ), 900(○) and 950°C (●). Continuous line: results predicted by the kinetic model

The reaction rate was very fast at all temperature and samples were oxidized back to the initial condition within 12 s at all temperatures. At lower temperatures the degree of conversion was slightly less than 1. This was due to the low degree of conversion reached in the previous reduction period. Further, it was observed that the oxidation reaction rate was a function of the O_2 concentration and reaction temperature. The reaction order n for oxidation reaction was obtained by the slope of the plot of ln (dX_o/dt) vs. ln (C_{O2}), (Figure 33). The slope was about 0.65, which is the reaction order with respect to oxygen.

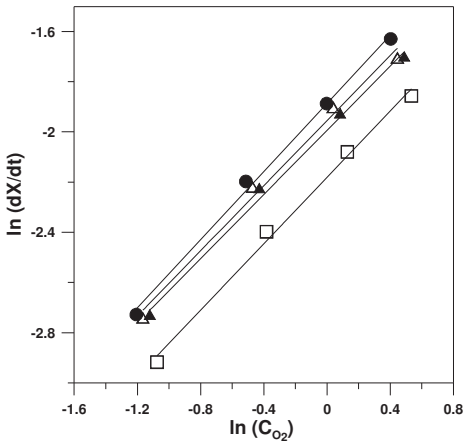

Figure 33: ln (dX_o/dt) as a function of ln (C_{O2}) to obtain the order of reaction for oxidation and the value k_o^* at different temperatures 800(□), 850(▲), 900(Δ) 950(●)

The Arrhenius plot obtained from the oxidation reaction data is given in Figure 30b. The energy of activation obtained from the Arrhenius plot was 19.5 kJ/mol and the pre-exponential factor $k_{0,o}$ found was 1.04 m^3 $mol^{0.65}$ s^{-1}. The kinetic constant k_o can be found by using the activation energy and pre-exponential factor.

The kinetic parameters obtained were used to predict the experimental data following the linear model. Only the chemical reaction was used as resistance controlling the reaction. The model results fit reasonably with the experimental result using chemical resistance controlling the global reaction rate (Figures 31 and 32).

7.4.3 Recirculation rate and solid inventory for the Mn_3O_4/Mg-ZrO_2 oxygen carrier

The reaction of Mn-based oxygen carriers with methane is endothermic and there will be a temperature drop in the fuel reactor. Figure 34 shows the decrease in temperature as a function of the incremental conversion, ΔX_S in the reactors. To avoid large temperature drops, the recirculation rate should not be too low. For example, if a limit in the temperature decrease of 50 ºC is imposed, the incremental conversion should be at maximum ΔX_S= 0.54 and the recirculation rate of the oxygen carrier per MW_f of CH_4 was 5.3 kg s^{-1} MW_f^{-1}.

The recirculation rate in the circulating fluidized bed also depends on the operational conditions and riser configuration. The value of the riser area in the CLC process for combustion of methane obtained is 0.18-0.35 m^2/MW_f. Taking a value of 0.2 m^2/MW_f as an average of the cross-section area of the riser, S_r, the solid flow can be calculated as

$$G_S = \frac{\dot{m}_{OC}}{S_r} \tag{25}$$

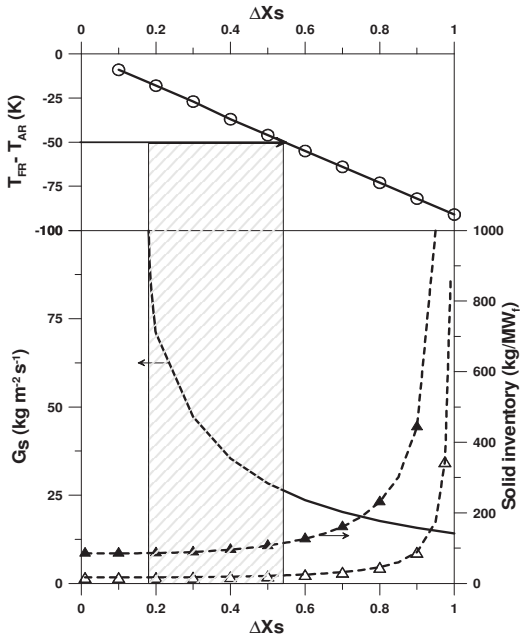

Figure 34: Solid circulation rate, solid inventory [$m_{OC,FR}$ (▲), $m_{OC,AR}$ (Δ)] and temperature difference between the air and fuel reactor as a function of solid conversion variation between the fuel and air reactor for the Mn_3O_4/Mg-ZrO_2 oxygen carrier

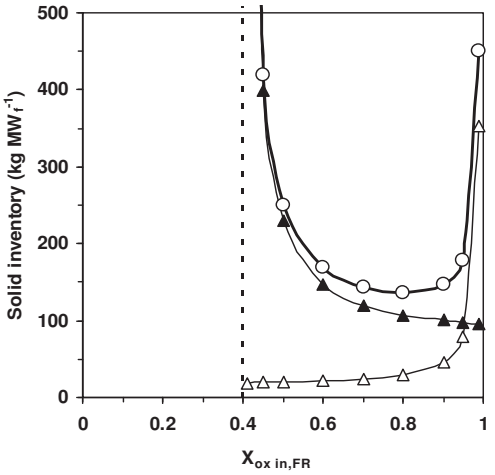

Figure 35: Optimum solid inventory for Mn_3O_4/Mg-ZrO_2 in the CLC reactors system. $m_{OC,FR}$ (▲), $m_{OC,AR}$ (Δ) and m_{total} (○).

The values of G_S reported in the literature are between 20 and 100 kg m^{-2} s^{-1}. Figure 34 shows the G_S and temperature difference in the air and fuel reactors as a function of ΔX_S for the Mn_3O_4/Mg-ZrO_2 oxygen carrier using methane as fuel. It can be seen that at higher values of ΔX_S there is a large temperature drop in the fuel reactor and a lower ΔX_S, the circulation rate is too high. To operate the fuel reactor at a sufficient temperature with a reasonable circulation rate the ΔX_S should be between 0.18-0.54. An adequate value for continuous systems could be a recirculation rate to obtain ΔX_S= 0.4. At these conditions, the value of G_S found was 35.4 kg m^{-2} s^{-1} for the Mn_3O_4/Mg-ZrO_2 oxygen carrier used in this work, which can be accomplished in the available riser. The solid inventory increase with increasing ΔX_S; however, the optimum solid inventory found was 135 kg/MW_f with a conversion difference of 0.4 between the air and fuel reactor (Figure 35). The method for calculating of solid inventory can be found in detail in paper IV.

8. Discussion

The present thesis deals with two chemical-looping processes CLC and CLR. Both methods involve the capture of carbon dioxide for sequestration, and since the CO_2 can be obtained in relatively pure form inherently in the process, there is not much energy expended for the separation. However, there are some fundamental differences between the two processes: In CLC, full conversion of fuel, in this case natural gas, to the oxidation products CO_2 and H_2O is required from the fuel reactor. In CLR partial oxidation of natural gas is desired in the fuel reactor and thus a considerable part of the outlet gas will be composed of CO and H_2. The oxygen carrier will supply oxygen to the fuel in both CLC and CLR, but the characteristics of the oxygen carrier may be different. In CLC it is important that the oxygen carrier is able to convert a substantial part of the natural gas to CO_2 and H_2O, whereas in CLR the oxygen carrier should be able to completely convert the CH_4, although a complete thermodynamic conversion to CO_2 and H_2O is not necessary. The first paper in this thesis focused on chemical-looping reforming. At the time when this study was initiated only limited work had been done, primarily by Ryden and Lyngfelt on the process [32], and no data was available on the oxygen carrier reactivity. Thus, a study was carried out in a batch fluidized bed reactor, where oxygen carriers based on Ni, Mn, Fe and Cu were evaluated specifically in relation to CLR. Similar type of experiments had earlier been done for evaluation of oxygen carriers for CLC, but here the focus was to asses the outlet composition of gases which may be viable in a CLR process. The oxygen supplied ratio o was used to quantify the outlet gas compositions, see equation 13. A high value of o signifies that the outlet products are combustion products; CO_2 and H_2O, while a lower value would mean that part of the products are CO and H_2. The oxygen supplied ratio is seen for CuO/SiO_2 and NiO/SiO_2 in Figure 11. It can be seen that o is high in the initial part of the reduction due to complete reaction to the oxidation products CO_2 and H_2O, i.e. the products, which are desired in regular CLC. As the reaction proceeds to lower degree of oxide conversion, the oxygen supplied ratio also decreases. However, as can be seen in Figure 6(a) and 11, a significant amount of methane is released from the reactor at low degree of conversion for Fe and Cu. To compare the outlet concentration of gaseous products for the tested oxygen carriers, Table 7 shows the concentrations when the oxygen supplied ratio o is equal to 1, i.e. half the oxygen needed for complete combustion is added to the gas phase. The data is taken from experiments conducted with Fe and Mn at 950 °C, whereas Cu and Ni at 800 °C.

Table 7 Outlet gas concentration at o=1 for different oxygen carriers tested in the fluidized-bed reactor

Oxygen Carriers	Outlet gas concentration (%)			
	CH_4	**CO_2**	**H_2**	**CO**
Fe_2O_3/SiO_2	61	18.9	13.8	6.3
Mn_2O_3/SiO_2	58	25	13.5	3.5
CuO/SiO_2	71.5	25.5	1.8	1.2
NiO/SiO_2	0.5	5.3	72.7	21.5

Clearly, in comparison with the other oxygen carriers, a very minor amount of CH_4 is released from the reactor with Ni compared to the other oxygen carriers when the oxygen supplied ratio is 1. Further, only Ni based oxygen carrier showed high degree of selectivity toward H_2 (Figure 11b). In a real process it is a great advantage if the methane conversion is high, the current experiments suggest that only nickel is a viable candidate of the tested metal oxides. However, recent experiments by Johansson et al. show that perhaps the combination of small amounts of nickel oxide particles together with iron oxide particles may provide high methane conversion and thus perhaps be possible to use in CLR [107].

There was a limited amount of work done in the literature using SiO_2 as a support for oxygen carriers when the project was initiated [81]. Of the SiO_2 supported carriers tested in the fluidized bed and TGA reactor, Fe_2O_3 and Mn_2O_3 carriers showed poor reactivity and the reactivity of these oxygen carriers decreased as a function of cycle, most probably due to the formation of metal silicates as a result of interaction between active metal oxide and inert phase. The silicates of Mn and Fe were found in XRD analysis of the reacted particles from the fluidized bed reactor (Table 5). It is likely that both Fe_2O_3/SiO_2 and Mn_2O_3/SiO_2 are not feasible oxygen carriers to be used in CLC and CLR unless the metal oxide-support interaction is hindered in some way. Also a major decrease in the reactivity was also seen for NiO/SiO_2 at 950 °C. This was due to the agglomeration of active phase on the support at higher temperature (Figure 13) but may also be due to silicate formation. However, this decrease in reactivity was avoided for NiO/SiO_2 at lower temperature i.e. at 800°C. Further, tests with NiO/SiO_2 particles prepared using freeze granulation do not show such deactivation, even at temperatures as high as 1000°C, see appendix.

Metal oxides supported on $MgAl_2O_4$ showed high reactivity during reduction and oxidation (Paper II). However, manganese oxide on $MgAl_2O_4$ showed a lower degree of conversion, which was attributed to the formation of manganese aluminates during the sintering of the fresh oxygen carrier and was seen in XRD analysis of fresh sample. $NiO/MgAl_2O_4$ showed the highest reaction rate both during reduction and oxidation and thus was identified as a promising oxygen carrier for CLC and CLR.

The second part of the thesis, i.e. paper III and IV, is focused on a kinetic determination for particles of $NiO/MgAl_2O_4$ and $Mn_3O_4/Mg\text{-}ZrO_2$. These were selected for kinetic studies due to the excellent reactivity shown in different studies [24, 27, 64, 74] including good performance in a continuous 300 W CLC and CLR unit [24, 25, 27]. Both $NiO/MgAl_2O_4$ and $Mn_3O_4/Mg\text{-}ZrO_2$ were prepared by freeze granulation and contains active metal oxide content of 60% and 40% respectively. The reactivity experiments were conducted in a TGA with CH_4 and O_2 used as reducing and oxidizing gas respectively. It was found that both the reduction and oxidation rates were dependent on the concentration of reacting gases and reaction temperatures for both oxygen carriers.

The reaction order for $NiO/MgAl_2O_4$ with CH_4 and O_2 was 0.4 and 1 respectively. Abad et al. investigated a carrier based on NiO with Al_2O_3 and found reaction order of 0.8 and 0.2 for CH_4 and O_2 respectively [80]. Readman et al. also investigated NiO on $NiAl_2O_4$ finding the values of the reaction order to be 0.74 and 1 for CH_4 and O_2 respectively [106]. The two types of particles are clearly different. This difference in the values of reaction order may be due to Mg addition in the oxygen carrier used in this work. The reaction order for $Mn_3O_4/Mg\text{-}ZrO_2$ with CH_4 and O_2 was 1 and 0.65 respectively. There has not been any investigation pf the kinetics for Mn-based oxygen carriers. However, the reaction order for most other oxygen carriers are in the range of 0.4-1.3 for the reduction and mostly 1 for oxidation [80, 87]. Thus

reaction order found for Mn_3O_4/Mg-ZrO_2 oxygen carrier in this work is in the range found for other oxygen carriers in the literature.

The activation energies for reduction and oxidation were 114 and 40 kJ/mol respectively, for NiO/$MgAl_2O_4$, whereas for Mn_3O_4/Mg-ZrO_2 the activation energies were 119 and 19 kJ/mol respectively. The activation energy for these two investigated oxygen carriers is rather high in comparison with those found for the previous investigated oxygen carriers [37, 80, 87, 105]. The high activation energy for the reduction reaction for the two oxygen carriers may be due to the addition of Mg, which increases the needed reduction temperature [79], which may increases the activation energy of the reaction.

The solid inventory needed in a CLC system is inversely proportional to the reactivity of the metal oxide with fuel and oxygen. The reactivity data and kinetic parameters obtained for NiO/$MgAl_2O_4$ and Mn_3O_4/Mg-ZrO_2 were used to estimate the solid inventory needed in a CLC system. For NiO/$MgAl_2O_4$ oxygen carrier the conversion variation between the air and fuel reactor was limited by the endothermic reaction in the fuel reactor. To operate the air and fuel reactors at 1000 and 950 °C respectively, maximum solid conversion difference between the two reactors was 0.18. For NiO/$MgAl_2O_4$ oxygen carrier the minimum solid inventory with a solid conversion of ΔX_S=0.18, is 22 kg/MW_f. This is a very small amount of material and should be compared with the amount of Ni-based oxygen carriers calculated by other authors. Mattisson et al. investigated NiO/Al_2O_3 prepared by impregnation in a TGA and found that the total solid inventory needed for CLC is 620 kg/MW [68]. NiO/$MgAl_2O_4$ oxygen carrier prepared by impregnation needed an inventory of 125-175 kg/MW, depending on the mass based conversion difference $\Delta\omega$ obtained in the reactor system [74]. However, these authors assumed first order reaction with average CH_4 and O_2 concentration of 10 and 5% in fuel and air reactor respectively. Also the active NiO content in these particles was below 30 %. Cho et al. studied freeze-granulated NiO on alumina support in a laboratory fluidized bed reactor and found that 57-162 kg/MW oxygen carrier is needed in the fuel reactor depending on the mass based solid conversion achieved during reduction [56]. Abad et al. found an inventory of 45 kg/MW_f of freeze granulated NiO on alumina support with an active MeO content of 40 wt% [80]. Thus, it is clear that the oxygen carrier investigated in this work has high promise. The fact that the oxygen carrier has also been used successfully in a continuous operation for both CLC and CLR, confirms the promise of the particles [25, 27]. However, it is important that similar particles can be produced using commercial production methods such as spray drying and commercial raw materials.

The second oxygen carrier i.e. Mn_3O_4/Mg-ZrO_2 also showed a good promise with an optimal solids inventory of 135 kg/MW_f, when the air and fuel reactors were operated at 1000 and 950 °C respectively. There are no published data available regarding Mn-based oxygen carriers and therefore the amount of oxygen carrier calculated in this work can be compared with the other commonly used oxygen carriers for CLC. The solid inventories for Ni-based oxygen carriers found in literature are in the range 45-620 kg/MW_f [68, 80] . The amount of oxygen carrier needed varies because of the preparation method, active metal loading, different assumptions and method used in the calculations. The solid inventories for the Cu-based oxygen carrier found in the literature are in the range 125-420 kg/MW_f [68, 74]. Garcia et al. found an inventory of 133 kg/MW_f for CuO/Al_2O_3 oxygen carrier prepared by impregnation containing 10 wt% active MeO content [87]. For Fe-based oxygen carriers the amount of bed material needed in CLC system is rather high because of the lower reactivity of iron oxide. The inventories for the Fe-carrier found in literature are in the range 220-1200 kg/MW_f [74, 80]. Although more amount of material is needed for the Mn-based oxygen

carrier in comparison to Ni-based oxygen carrier, the inventory is low in comparison to almost all earlier investigated particles in the literature. Mn-based oxygen carriers are also cheaper and less toxic than Ni carrier. Furthermore, because of the lower melting point of Cu and lower reactivity of Fe_2O_3 in addition to thermodynamic limitations, Mn-based oxygen carrier may be an attractive option for CLC.

9. Conclusions

This thesis deals with two chemical-looping technologies called chemical-looping combustion and chemical-looping reforming. CLC is an unmixed type of combustion, in which CO_2 is inherently separated from the rest of the flue gases with only small energy losses. CLR is a process for integrated hydrogen and power production from natural gas with CO_2 capture. The technique CLR is based on CLC, and an oxygen carrier is used to transfer oxygen and heat between the air and fuel reactor. Thus a stream of H_2, CO, CO_2 and H_2O that is undiluted with N_2 is obtained from the fuel reactor. A total of eleven different oxygen carriers based on the metals Fe, Ni, Cu and Mn have been tested using batch fluidized beds and/or TGA reactors. Eight of the oxygen carriers were prepared by impregnation of the active metal oxide on a support, and three systems were prepared by freeze granulation. In addition; reduction and oxidation kinetics of two promising oxygen carriers for CLC, $NiO/MgAl_2O_4$ and Mn_3O_4/Mg-ZrO_2 were investigated using CH_4 and air in a TGA.

The main conclusions from the work in this thesis are:

- Of the investigated metal oxides supported on $MgAl_2O_4$ and SiO_2, NiO and CuO oxygen carrier showed high reactivity under both reducing and oxidizing conditions.

- NiO has the highest selectivity toward H_2 of the investigated metal oxides and thus may be the most feasible oxygen carrier for CLR.

- Fe_2O_3/SiO_2 and Mn_2O_3/SiO_2 showed signs of deactivation as a function of cycle in the fluidized bed. This deactivation was attributed to the formation of irreversible metallic silicates.

- All the $MgAl_2O_4$-supported metal oxides are very reactive with methane and air and no deactivation was seen as a function of cycle. However manganese supported on $MgAl_2O_4$ showed a low degree of conversion.

- Two interesting oxygen carriers, based on $NiO/MgAl_2O_4$ and Mn_3O_4/Mg-ZrO_2 prepared by freeze granulation were investigated under alternating oxidizing and reducing conditions in a TGA. The reactivity was a function of reacting gas concentration and temperature.

- $NiO/MgAl_2O_4$ may not be feasible to be used at temperature below 900 °C.

- The activation energy found for $NiO/MgAl_2O_4$ and Mn_3O_4/Mg-ZrO_2 was rather high when compared with that reported in the literature for different oxygen carriers. This effect is may be due to the Mg addition in the particles

- From the kinetic data it was possible to establish design data for CLC. To operate the air and fuel reactors of the CLC system with the $NiO/MgAl_2O_4$ oxygen carrier, the

solid conversion difference between the two reactors should not be more than 0.18, with a recirculation rate of 4.15 kg s^{-1} MW_f^{-1}.

- The total solid inventory for the $NiO/MgAl_2O_4$ oxygen carrier varies with the solid conversion at the inlet of the fuel and air reactors. The minimum solid inventory found was 22 kg/MW_f.

- The optimum solid inventory found for Mn_3O_4/Mg-ZrO_2 was 135 kg/MW_f and the recirculation rate was 7.12 kg s^{-1} $MW_f^{-}1$, when ΔX_s=0.4.

- The results from the kinetic determination together with earlier experience with the Ni- and Mn-based oxygen carriers show that these may be the good candidates as oxygen carriers in a real CLC system, provided that the production method can be scaled up.

10. Notations

b= Stoichiometric factor for the reaction, mol solid reactant

C_g= gas concentration mol/m^3

D_e= effective diffusion coefficient

E = activation energy, kJ mol^{-1}

G_S= specific solids circulation rate, kg m^{-2} s^{-1}

K = equilibrium constant for water shift reaction.

k = chemical reaction rate constant, mol^{1-n} m^{3n-2} s^{-1}

k_0= pre-exponential factor of the chemical reaction rate constant, mol^{1-n} m^{3n-2} s^{-1}

m = actual mass of the oxygen carrier, g

m_{red} = mass of the sample in reduced form, g

m_{ox} = mass of the sample when it is fully oxidized, g

$m_{OC,FR}$= solid inventory, in the fuel reactor , (kg OC) MW_f^{-1}

$m_{OC,AR}$= solid inventory, in the air reactor , (kg OC) MW_f^{-1}

m_{total}=total solid inventory, as fully oxidized oxygen carrier, (kg OC) MW_f^{-1}

$\dot{m}_{OC}$ = circulation rate of fully oxidized oxygen carrier, (kg OC) s^{-1} MW_f^{-1}

M_o = moles of active oxygen in the fresh oxygen carrier, mol

M_i = molar mass of gas species i, kg/kmol

n_{in} = molar flow rates of the gas entering the reactor, mol/s

n_{out} = molar flow rates of the gas leaving the reactor, mol/s

n = reaction order

o = oxygen supplied ratio

$p_{i,out}$ = partial pressure of gas i exiting the reactor after removal of water, Pa

$p_{i,in}$ = partial pressure of gas i entering the reactor, Pa

P_{tot} = total pressure, Pa

R_o = oxygen ratio i.e. the maximum mass fraction of oxygen that can be transferred between the air and fuel reactor.

r_g = grain radius, m

Sr= cross section area of the riser per MW_f, m^2 MW_f^{-1}

t = time, s

t_0 = time for start of the period, s

t_1 = time for finish of the period, s

X = conversion of oxygen carrier or the degree of oxidation

X_i = conversion as a function of time for period i

X_{i-1} = conversion after the preceding period

X_s = solid conversion

Greek letters

τ= time required for complete conversion of the particles, s

ω = mass-based conversion of oxygen carrier

ΔX_s = variation of the solid conversion between the two reactors

ρ_m = molar density of the reacting material, mol m^{-3}

11. Acknowledgements

I would like to thank the following persons and organizations:

My supervisor Associate Professor Tobias Mattisson for all help, encouragement and support, valuable discussions, and reading my papers and the thesis; tusen tack, Tobias.

Professor Krister Holmberg and Associate Professor Börje Gevert for providing me the opportunity to perform my graduate studies at the Department of Applied Surface Chemistry.

Dr. Alberto Abad for giving useful suggestions for the experimental work, for reading the papers and all his help during my PhD work.

Professor Anders Lyngfelt for reading my papers and arranging Nordic CO_2 course.

All members of CLC group at Chalmers and especially Marcus Johansson for helping with fluidized bed reactor experiments and for valuable discussions.

All people at the Department of Teknik and Design Växjö University, especially Dr. Mikael Strand for his magic solutions whenever there was some problem.

Hussam and Bagas for scientific discussions and being good friends.

Thomas and Aslan for their help with computer.
Ann for doing all paper work and many other official things.

All colleagues at Applied Surface Chemistry for creating a pleasant working environment.

I would like to thank Ångpanneföreningens Forskningsstiftelse, Nordisk Energiforskning and CF Miljöfond for the financial support.

Last but not least, I would like to thank my family and relatives for their love and support.

12. References

1. *Third Assessment Report of the Intergovernmental Panel on Climate Change (IPCC). Climate Change: The Scientific Basis, ed. J.T. Houghton, et al. :Cambridge University Press, UK.* 2001.
2. Azar, C., Lindgren, K., Andersson, B. *Global energy scenarios meeting stringent CO_2 constraints- cost effective fuel choices in the transportation sector.* Energy policy, 2003. **31**: p. 961-976.
3. *IPCC special report on carbon dioxide capture and storage.* Cambridge University Press, 2005.
4. Audus, H., O. Kaarstad, and G. Skinner. *CO_2 capture by pre-combustion decarbonisation of natural gas.* Proceedings of the 4th International Conference on Greenhouse Gas Control Technologies, Interlaken, 1998: p. 557-562.
5. Adanez, J., Gyan, P., Celaya, J., de diego,L.,Garcia-Labiano, F., Abad, A. *Chemical Looping Combustion in a 10 kWth Prototype Using a CuO/Al_2O_3 Oxygen Carrier: Effect of Operating Conditions on Methane Combustion.* Ind. Eng. Chem. Res., 2006. **45**: p. 6075-6080.
6. Lyngfelt, A., Kronberger, B., Adanez, J., Morin, J.-X, Hurst, P. *Development of oxygen carrier particles for chemical-looping combustion. Design and operation of a 10 kW chemical-looping combustor.* Proceedings of the 7th International Conference on Greenhouse Gas Control Technologies, Vancouver 2004.
7. Lyngfelt, A., Leckner, B., Mattisson, T. *A fluidized-bed combustion process with inherent CO_2 separation; application of chemical-looping combustion.* Chem. Eng. Sci., 2001. **56**: p. 3101-3113.
8. Ryu, H.-J., G.-T. Jin, and C.-K. Yi. *Demonstration of inherent CO_2 separation and no NOx emission in a 50 kW chemical-looping combustor: continuous reduction and oxidation experiment.* Proceedings of the 7th International Conference on Greenhouse Gas Control Technologies, Vancouver 2004.
9. *IEA Greenhouse gas R&D Programme, Putting carbon back into the ground, February 2001, ISBN 1898373280.*
10. Lindeberg, E. *Future large-scale use of fossil energy will require CO_2 sequestering and disposal.* in *Minisymposium on Carbon Dioxide Capture and Storage, Chalmers University of Technology Göteborg, October 1999.*
11. Holt, T., Lindeberg, E. *Carbon dioxide from industrial sources as injection gas in oil reservoir.* Energy Convers. Manage, 1993. **34**: p. 1189-1196.
12. Lindeberg, E. and S. Holloway. *The next steps in geo-storage of carbon dioxide.* Proceedings of the 4th International Conference on Greenhouse Gas Control Technologies, Interlaken, 1998: p. 145-150.
13. Lindeberg, E., Bergmo, P. *The long-term fate of CO_2 injected into an aquifer.* 6th International Conference on Greenhouse Gas Control Technologies, Kyoto, Japan 2003.
14. Lyngfelt, A., Leckner, B. *Technologies for CO_2 separation.* in *Minisymposium on Carbon Dioxide Capture and Storage, Chalmers University of Technology Göteborg, October 1999.*
15. Anheden, M., Svedberg G. *Exergy analysis of chemical-looping combustion system.* Energy Convers. Manage, 1998. **39**: p. 1967-1980.
16. Ishida, M., D. Zheng, and T. Akehata. *Evaluation of a chemical-looping-combustion power-generation system by graphic exergy analysis.* Energy - the International Journal, 1987. **12**: p. 147-154.
17. Richter, H. and K. Knoche. *Reversibility of combustion processes.* ACS Symp. Ser, 1983. **235**: p. 71-86.
18. Ishida, M. and H. Jin, *A novel chemical-looping combustor without NOx formation.* Ind.Eng.Chem.Res., 1996. **35**: p. 2469-2472.
19. Johansson, E., Lyngfelt, A., Mattisson, T., Johnsson, F. *A circulating fluidized bed combustor system with inherent CO_2 separation - Application of chemical looping combustion.* 7th Int. Conf. on Circulating Fluidized Beds, Niagara Falls, Ontario, May 5-7, 2002: p. 717-724.
20. Johansson, E., Lyngfelt, A., Mattisson, T., Johnsson, F. *Gas leakage measurements in a cold model of an interconnected fluidized bed for chemical-looping combustion.* Powder Techn., 2003. **134**: p. 210-217.
21. Kronberger, B., Lyngfelt, A., Löffler, G., Hofbauer, H. *Design and hydrodynamic testing of a 10-kW prototype for continuous chemical-looping combustion.* Ind.Eng.Chem.Res, 2005. **44**: p. 546-556.
22. Lyngfelt, A., Thunman, H. *Construction and 100 h of operational experience of a 10-kW chemical-looping combustor*, in *Carbon Dioxide Capture for Storage in Deep Geologic Formations - Results from the CO_2 Capture Project, Volume 1 - Capture and Separation of Carbon Dioxide From Combustion Sources.* 2005, Elsevier Science: London. p. 625-645.
23. Abad, A., Mattisson, T., Lyngfelt, A., Johansson, M. *The use of iron oxide as oxygen carrier in a chemical-looping reactor.* Fuel, 2007. **86**: p. 1021-1035.
24. Abad, A., Mattisson, T., Lyngfelt, A., Ryden, M. *Chemical-looping combustion in a 300 W continuously operating reactor system using a manganese-based oxygen carrier.* Fuel 2006. **85**: p. 1174-1185.

25. Johansson, E., Mattisson, T., Lyngfelt, A. *A 300 W laboratory reactor system for chemical-looping combustion with particle circulation.* Fuel, 2006. **85**: p. 1428-1438.
26. Johansson, E., Mattisson, T., Lyngfelt, A., Thunman, H. *Combustion of syngas and natural gas in a 300 W chemical-looping combustor.* Chem. Eng. Res. Des., 2006. **84**: p. 819-827.
27. Ryden, M., Lyngfelt, A., Mattisson, T. *Synthesis gas generation by chemical-looping reforming in continuously operating laboratory reactor.* Fuel 2006. **85**: p. 1631-1641.
28. Kronberger, B., Johansson, E., Löffler, G., Mattisson, T. Lyngfelt, A., Hofbauer, H., *A two-compartment fluidized bed reactor for CO_2 capture by chemical-looping combustion.* Chem.Engng.Techn., 2004. **27**: p. 1318-1326.
29. Mattisson, T., Lyngfelt, A. *Applications of chemical-looping combustion with capture of CO_2. Second Nordic Minisymposium on CO_2 capture and storage, Göteborg, Sweden 2001.*
30. Mattisson, T., Zafar, Q., Lyngfelt, A., Gevert, B. *Integrated hydrogen and power production from natural gas with CO_2 capture*. 15th World Hydrogen Energy Conference, Yokohama, June 27- July 2 2004.
31. Ryden, M. *Hydrogen Production with Carbon Dioxide Capture by Reforming of Natural Gas using Chemical-Looping Technologies.* Licentiate Thesis Chalmers University of Technology, Göteborg Sweden, 2006.
32. Rydén, M., Lyngfelt, A. *Hydrogen and power production with integrated carbon dioxide capture by chemical-looping reforming.* Proceedings of the 7th International Conference on Greenhouse Gas Control Technologies, Vancouver 2004.
33. Rydén, M. and A. Lyngfelt. *Using steam reforming to produce hydrogen with carbon dioxide capture by chemical-looping reforming.* J. Hydrogen Energy 2006. **31**: p. 1271-1283.
34. Mattisson, T., Lyngfelt, A. *Capture of CO_2 using chemical-looping combustion.* First Biennial Meeting of the Scandinavian-Nordic Section of the Combustion Institute, April 18-20, Göteborg, Sweden, 2001.
35. Ishida, M. and H. Jin. *A novel combustor based on chemical-looping reactions and its reaction kinetics.* J. Chem. Eng. Japan, 1994. **27**: p. 296-301.
36. Ishida, M. and H. Jin. *CO_2 recovery in a power plant with chemical-looping combustion.* Energy Convers. Mgmt, 1997. **38**: p. S187-S192.
37. Ishida, M., H. Jin, and T. Okamoto. *A fundamental study of a new kind of medium material for chemical-looping combustion.* Energy & Fuels, 1996. **10**: p. 958-963.
38. Ishida, M., H. Jin, and T. Okamoto. *Kinetic behaviour of solid particle in chemical-looping combustion: suppressing carbon deposition in reduction.* Energy & Fuels, 1998. **12**: p. 223-229.
39. Ishida, M., Takeshita, K.,Suzuki, K.,Ohba, T. *Application of Fe_2O_3-Al_2O_3 composite particles as solid looping material of the chemical-looping combustor.* Energy & Fuels, 2005. **19**: p. 2514-2518.
40. Ishida, M., M. Yamamoto, and T. Ohba. *Carbon dioxide recovery in a power plant with chemical-looping combustion.* Technology, 2000. **7S**: p. 3-12.
41. Ishida, M., M. Yamamoto, and Y. Saito. *Experimental works on innovative chemical-looping combustor.* ECOS'99, International Conference on Efficiency, Costs, Optimization, Simulation and Environmental Aspects of Energy Systems, Tokyo, June 8-10, , 1999: p. 306-310.
42. Jin, H. and M. Ishida. *A new advanced IGCC power plant with chemical-looping combustion.* Proceedings of Thermodynamic Analysis and Improvement of Energy Systems (TAIES'97) June 10-13, Beijing, 1997: p. 548-553.
43. Jin, H. and M. Ishida. *A novel gas turbine cycle with hydrogen-fueled chemical-looping combustion.* Int. J. of Hydrogen Energy, 2000. **25**: p. 1209-1215.
44. Jin, H. and M. Ishida. *Reactivity study on a novel hydrogen fueled chemical-looping combustion.* Int. J. of Hydrogen Energy, 2001. **26**: p. 889-894.
45. Jin, H. and M. Ishida. *A new type of coal gas fueled chemical-looping combustion.* Fuel, 2004. **83**: p. 2411-2417.
46. Jin, H., T. Okamoto, and M. Ishida. *Development of a novel chemical-looping combustion: synthesis of a solid looping material of $NiO/NiAl_2O_4$.* Ind.Eng.Chem.Res, 1999. **38**: p. 126-132.
47. Jin, H., T. Okamoto, and M. Ishida. *Development of a novel chemical-looping combustion: synthesis of a looping material with a double metal oxide of CoO-NiO.* Energy & Fuels, 1998. **12**: p. 1272-1277.
48. Nakano, Y., Wamoto, S., Maeda, T., Ishida, M., Akehata, T. *Characteristics of reduction and oxidization cyclic process by use of αFe_2O_3 medium.* Iron & Steel Journal of Japan, 1986. **72**: p. 1521-1527.
49. Jin, H. and M. Ishida. *Reactivity study on natural-gas-fueled chemical-looping combustion by a fixed-bed reactor.* Ind.Eng.Chem.Res, 2002. **41**: p. 4004-4007.
50. Ishida, M., M. Yamamoto, and T. Ohba. *Experimental results of chemical-looping combustion with $NiO/NiAl_2O_4$ particle recirculation at 1200 °C.* Energy Convers. Mgmt, 2002. **43**: p. 1469-1478.

51. Copeland, R., Alptekin, G., Cesario, M., Gebhard, S. Gershanovich, Y. *A novel CO_2 separation system*. The 8th International Symposium on Transport Phenomena and Dynamics of Rotating Machinery. Honolulu, Hawaii, USA, 2000.
52. Copeland, R., Alptekin, G., Cesario, M., Gebhard, S., Gershanovich, Y. *A novel CO_2 separation system First National Conference on Carbon Sequestration, National Energy Technology Laboratory (NETL), Washington, May 15-17, 2001*.
53. Copeland, R., Alptekin, G., Cesario, M., Gebhard, S. Gershanovich,Y. *Sorbent Energy Transfer System (SETS) for CO_2 Separation with High Efficiency. 27th International Conference on Coal Utilization & Fuel Systems, Clearwater, Florida 2002.*
54. Cho, P. *Development and Characterization of Oxygen-Carrier Materials for Chemical-Looping Combustion, PhD Thesis*. 2005, Göteborg, Sweden: Department of Chemical and Biological Engineering, Environmental Inorganic Chemistry, Chalmers University of Technology.
55. Cho, P., Mattisson, T., Lyngfelt, A. *Reactivity of iron oxide with methane in a laboratory fluidized bed - Application of chemical-looping combustion.* 7th Int. Conf. on Circulating Fluidized Beds, Niagara Falls, Ontario, May 5-7, 2002: p. 599-606.
56. Cho, P., Mattisson, T., Lyngfelt, A. *Comparison of iron-, nickel-, copper- and manganese-based oxygen carriers for chemical-looping combustion.* Fuel, 2004. **83**: p. 1215-1225.
57. Cho, P., Mattisson, T., Lyngfelt, A. *Carbon formation on nickel and iron oxide-containing oxygen-carriers for chemical-looping combustion.* Ind.Eng.Chem.Res, 2005. **44**: p. 668-676.
58. Cho, P., Mattisson, T., Lyngfelt, A. *Defluidization conditions for fluidized-bed of iron, nickel and manganese oxide containing oxygen-carriers for chemical-looping combustion.* Ind.Eng.Chem.Res., 2006. **45**: p. 968-977.
59. Johansson, M., *Selection of Oxygen-Carriers for Chemical-Looping Combustion Using Methane as Fuel, Lic.Eng. Thesis*. 2005, Göteborg, Sweden: Chalmers University of Technology Göteborg Sweden.
60. Johansson, M., Mattisson, T., Lyngfelt, A. *Investigation of Fe_2O_3 with $MgAl_2O_4$ for chemical-looping combustion.* Ind.Eng.Chem.Res., 2004. **43**: p. 6978-6987.
61. Johansson, M., Mattisson, T., Lyngfelt, A. *Use of $NiO/NiAl_2O_4$ particles in a 10 kW chemical-looping combustor.* Ind.Eng.Chem.Res. , 2006. **45**: p. 5911-5919.
62. Johansson, M., Mattisson, T., Lyngfelt, A. *Comparison of oxygen carriers for chemical-looping combustion.* International Symposium: Moving towards zero-emission plants, CRTH/ISTFA, Leptokarya Piera, Greece, June 20-22, 2005.
63. Johansson, M., Mattisson, T., Lyngfelt, A. *Comparison of oxygen carriers for chemical-looping combustion. Therm. Sci.*, 2006. **10**: p. 93-107.
64. Johansson, M., Mattisson, T., Lyngfelt, A. *Investigation of Mn_3O_4 with stabilized ZrO_2 for chemical-looping combustion.* Chem. Eng. Res.Des., 2006. **84**: p. 807-818.
65. Johansson, M., Mattisson, T., Lyngfelt, A. *Comparison of oxygen carriers for chemical-looping combustion of methane-rich fuels.* FBC Wien May 2006.
66. Mattisson, T., Johansson, M., Lyngfelt, A. *Multi-cycle reduction and oxidation of different types of iron oxide particles - Application to chemical-looping combustion.* Energy & Fuels, 2004. **18**(3): p. 628-637.
67. Mattisson, T., Johansson, M., Lyngfelt, A. *The use of NiO as an oxygen carrier in chemical-looping combustion.* Fuel, 2006. **85**: p. 736-747.
68. Mattisson, T., Järdnäs, A., Lyngfelt, A. *Reactivity of some metal oxides supported on alumina with alternating methane and oxygen - Application for chemical-looping combustion.* Energy & Fuels, 2003. **17**: p. 643-651.
69. Mattisson, T., Lyngfelt, A. *The use of iron oxide as an oxygen carrier in chemical-looping combustion of methane with inherent separation of CO_2 (in Swedish).* 1999. Eskilstuna: Energiting. Swedish National Energy Administration.
70. Mattisson, T., Lyngfelt, A., Cho, P. *The use of iron oxide as an oxygen carrier in chemical-looping combustion of methane with inherent separation of CO_2.* Fuel, 2000. **80**: p. 1953-1962.
71. Mattisson, T., Lyngfelt, A., Cho, P. *Possibility of using iron oxide as an oxygen carrier for combustion of methane with removal of CO_2 - Application of chemical-looping combustion.* Fifth International Conference on Greenhouse Gas Control Technologies, Cairns, Australia, 13th-16th August, 2000.
72. Zafar, Q. *Investigation of oxygen carrier materials for chemical-looping reforming. Licentiate Thesis Chalmers University of Technology Göteborg Sweden* 2005.
73. Zafar, Q., Mattisson, T., Gevert, B. *Integrated hydrogen and power production with CO_2 capture using chemical-looping reforming - redox reactivity of particles of CuO, Mn_2O_3, NiO, Fe_2O_3 using SiO_2 as a support.* Ind.Eng.Chem.Res. , 2005. **44**: p. 3485-3496.
74. Zafar, Q., Mattisson, T.,Gevert, B. *Redox investigation of some oxides of transition state metals Ni,Cu,Fe and Mn supported on SiO_2 and $MgAl_2O_4$.* Energy & Fuels, 2006. **20**: p. 34-44.

75. Mattisson, T., Zafar, Q., Johansson, M., Lyngfelt,A. *Chemical-looping combustion as a new CO_2 management technology.* 1st Regional Symposium on Carbon Management, Dhahran, Saudi Arabia 2006.
76. Ryu, H.-J., D.-H. Bae, and G.-T. Jin. *Effect of temperature on reduction reactivity of oxygen carrier particles in a fixed bed chemical-looping combustor.* Korean J. Chem. Eng., 2003. **20**(5): p. 960-966.
77. Ryu, H.-J.B., D-H., Han, K-H., Lee, S-Y., Jin, G-T., Choi, J-H. *Oxidation and Reduction Characteristics of Oxygen Carrier Particles and Reaction Kinetics by Unreacted Core Model.* . Korean J. Chem. Eng. , 2001. **18**(6): p. 831-837.
78. Ryu, H.-J.J., G.-T.Bae,D.-H. Yi,C.-K. *Continuous operation of a 50 kWth chemical-looping combustor: long-term operation with Ni- and Co-based oxygen carrier particles.* 5th China-Korea Joint Workshop on Clean Energy Technology, Qingdao University, China, October 25-28, 2004: p. 221-230.
79. Villa, R., C. Cristiani, G. Groppi, L. Lietti, P. Forzatti, U. Cornaro, and S. Rossini. *Ni based mixed oxide materials for CH_4 oxidation under redox cycle conditions.* J. of Molecular Catalysis A: Chemical, 2003. **204-205**: p. 637-646.
80. Abad, A., Adanez, J., García-Labiano, F., de Diego, L.F., Gayán, P., Celaya, J. *Mapping of the range of operational conditions for Cu-,Fe-, and Ni-based oxygen carriers in chemical-looping combustion.* Chem. Eng. Res. Sci, 2007. **62**(533-549).
81. Adánez, J., de Diego, L.F., García-Labiano, F.,Gayán, P.,Abad, A. *Selection of oxygen carriers for chemical-looping combustion.* Energy & Fuels, 2004. **18**: p. 371-377.
82. Adánez, J., García-Labiano, F., de Diego, L.F., Gayán, P., Abad, A., Celaya, J. *Development of oxygen carriers for chemical-looping combustion*, in *Carbon Dioxide Capture for Storage in Deep Geologic Formations - Results from the CO_2 Capture Project, Volume 1 - Capture and Separation of Carbon Dioxide From Combustion Sources.* 2005, Elsevier Ltd: Amsterdam. p. 587-604.
83. Adánez, J., de Diego, L.F. García-Labiano, F. Gayán, P. Abad, A., Celaya, J. *Characterization of oxygen carriers for chemical-looping combustion.* Proceedings of the 7th International Conference on Greenhouse Gas Control Technologies, Vancouver 2004.
84. Adánez, J., García-Labiano, F., de Diego, L.F.,Gayán, P.,Abad, A., Celaya, J. *Optimizing the fuel reactor for chemical looping combustion*. 2003.
85. de Diego, L.F., García-Labiano,F.,Adánez,J.,Gayán,P.,Abad,A.,Corbella,B.,Palacios,J. *Development of Cu-based oxygen carriers for chemical-looping combustion.* Fuel, 2004. **83**: p. 1749-1757.
86. de Diego, L.F., Gayán, P.,García-Labiano, F.,Celaya, J.,Abad, A.,Adánez, J. *Impregnated CuO/Al_2O_3 oxygen carriers for chemical-looping combustion: avoiding fluidized bed agglomeration.* Energy & Fuels, 2005. **19**: p. 1850-1856.
87. García-Labiano, F., de Diego, L.F., Adánez, J.,Abad, A.,Gayán, P. *Reduction and oxidation kinetics of a copper-based oxygen carrier prepared by impregnation for chemical-looping combustion.* Ind.Eng.Chem.Res., 2004. **43**: p. 8168-8177.
88. García-Labiano, F., de Diego, L.F., Adánez, J., Abad, A., Gayán, P. *Temperature variations in the oxygen carrier particles during their reduction and oxidation in a chemical-looping combustion system.* Chem. Eng. Sci., 2005. **60**: p. 851-862.
89. Corbella, B., de Diego, L.F., García-Labiano, F., Adánez, J., Palacios, J. *The performance in a fixed-bed reactor of copper-based oxides on titania as oxygen carriers for chemical-looping combustion of methane.* Energy & Fuels, 2005. **19**: p. 433-441.
90. Corbella, B., de Diego,L.F., García-Labiano,F., Adánez,J., Palacios,J. *Characterization study and five-cycle tests in a fixed-bed reactor of titania-supported nickel oxide as oxygen carriers for the chemical-looping combustion of methane.* Env.Sci.Techn., 2005. **39**: p. 5796-5803.
91. Corbella, B.M., de Diego,L.F, Garcia-Labiano, F., Adanez, J., and Palacios, J.M. *Characterization and Performance in a Multicycle Test in a Fixed-Bed Reactor of Silica-Supported Copper Oxide as Oxygen Carrier for Chemical-Looping Combustion of Methane.* . Energy & Fuels, 2006. **20**: p. 148-54.
92. Corbella, B.M., de Diego, L.F., Garcia-Labiano, F., Adanez, J.,Palacios, J.M. *Performance in a Fixed-Bed Reactor of Titania-Supported Nickel Oxide as Oxygen Carriers for the Chemical-Looping Combustion of Methane in Multicycle Tests.* Ind. Eng. Chem. Res. , 2006. **45**: p. 157-65.
93. Stobbe, E., Boer,B.de., Geus,J., *The reduction and oxidation behaviour of manganese oxides.* Catalysis Today, 1999. **47**: p. 161-167.
94. Mattisson, T., Johansson, M., Lyngfelt, A. *CO_2 capture from coal combustion using chemical-looping combustion – Reactivity investigation of Fe, Ni and Mn based oxygen carriers using syngas.* The Clearwater Coal Conference, Clearwater FL, 2006.
95. *Kunni, D. Levenspiel, O. Fluidization Engineering. 1991, 2nd Edition, Butterworth-Heinemann, p. 68-71.*
96. Kimura, S., Nakagawa, J-I., Tone, S., Otake, T. *The volume reaction model based on a second order rate equation and its application to a gas-solid reaction.* J. Chem. Eng. Japan, 1981. **14**(3): p. 190-195.

97. Levenspiel, O., *Chemical Reactor Omnibook.* OSU Bookstores, Corvallis, OR, 1996.
98. Park, J.Y., Levenspiel, O. *The cracking core model for the reaction of solid particles.* Chem. Eng. Sci., 1975. **30**: p. 1207-1214.
99. Ramachandran, P.A., Smith, J.M. *A single-pore model for gas-solid noncatalytic reactions.* AIChE Journal, 1977. **23**(353-361).
100. Ramachandran, P.A., Doraiswamy, L.K. *Modeling of noncatalytic gas-solid reactions.* AIChE Journal, 1982. **28**(6): p. 881-900.
101. Levenspiel, O., *Chemical Reaction Engineering 3rd edition John Wiley & Sons* 1999.
102. Snow, M.J.H., Longwell, J.P., Sarofim, A.F. *Direct sulfation of calcium carbonate.* Ind. Eng. Chem. Res., 1988. **27**: p. 268-273.
103. Zevenhoven, R., Yrjas, P., Huppa, M. *Sulfur dioxide capture under PFBC conditions: the influence of sorbent particles srtucture.* Fuel, 1998. **77**(4): p. 285-292.
104. García-Labiano, F., Adánez, J.,de Diego, L.F., Gayán, P., Abad, A. *Effect of pressure on behaviour of Copper-, Iron-, and Nickel-based oxygen carriers for chemical-looping combustion.* Energy & Fuels, 2006. **20**: p. 20-33.
105. Son, S.R., Kim., S.D. *Chemical-Looping Combustion with NiO and Fe_2O_3 in a thermobalance and ciculating fluidized bed reactor with double loops.* Ind. Eng. Chem. Res., 2006. **45**: p. 2689-2696.
106. Readman, J.E.O., A., Smith, J.B., Blom, R. *Chemical looping combustion using NiO/$NiAl_2O_4$: Mechanisms and kinetics of reduction -oxidation (Red-Ox) reactions from insitu powder X-ray Diffraction and Thermogravimetry experiments.* Energy & Fuels 2006. **20**: p. 1382-1387.
107. Johansson, M., Mattisson, T., Lyngfelt, A. *Creating a Synergy Effect by Using Mixed Oxides of Iron- and Nickel Oxides in the Combustion of Methane in a Chemical-Looping Combustion Reactor.* Energy & Fuels 2006. **20**: p. 2399-2407.

13. Appendix

Reactivity of freeze-granulated particles of NiO/SiO_2

Particles composed of 83 wt% NiO and 17 wt% SiO_2 were prepared using freeze granulation. The freeze granulation process was described in section 5.1.2. The particles were sintered at 1500°C for 6h. These particles were then tested under alternating oxidizing and reducing conditions in Setaram TAG 24S16, TGA using a gas composition of 10 % CH_4, 10 % H_2O, 5% CO_2 under reduction and 5%O_2 under oxidation at different temperatures.

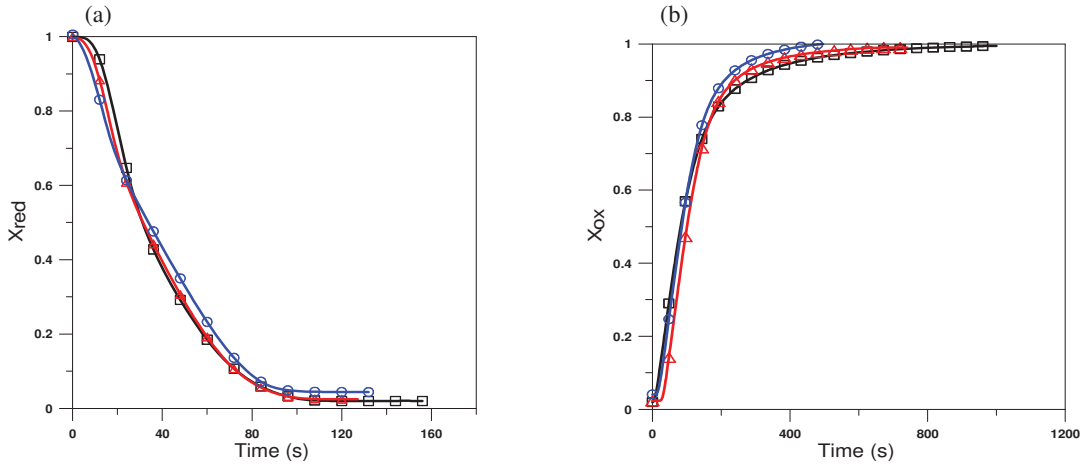

Figure A1: Conversion as a function of time **(a)** 2nd reduction period and **(b)** 3rd oxidation period for freeze granulated NiO/SiO_2 particles at 1000 °C (□), 950 °C (Δ), and 850 °C (○)

The conversion as a function of time is shown in Figure A1 for both reduction and oxidation at different temperatures. Clearly, both reduction and oxidation are fast initially at all temperatures and almost complete conversion is reached at all temperatures.

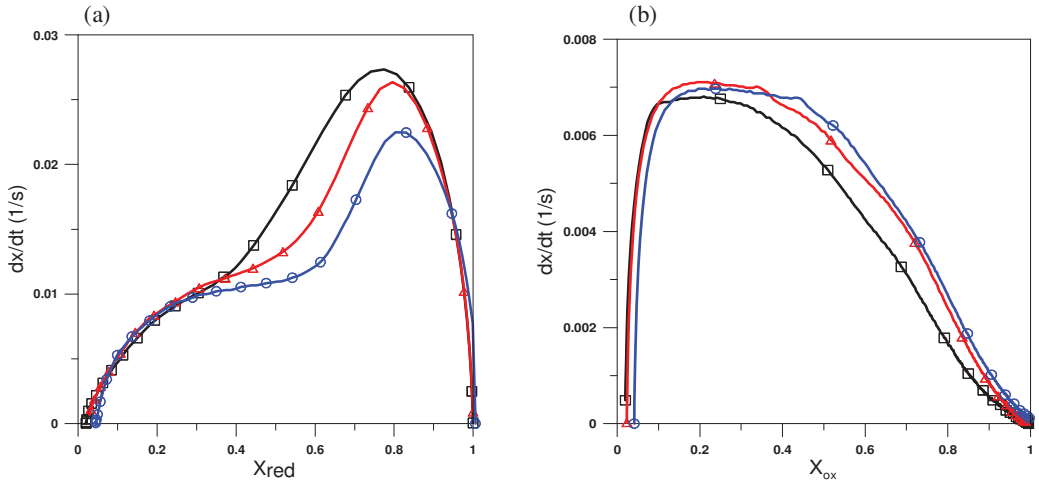

Figure A2: Reduction rate as a function of degree of conversion, X, for **(a)** 2nd reduction period and **(b)** 3rd oxidation period for freeze granulated NiO/SiO_2 at 1000 °C (□), 950 °C (Δ) and 850 °C (○).

Figure A2 shows the rate of reduction and oxidation, dX/dt, as a function of the conversion, X, for different temperatures. For the reduction the initial rates are slightly dependent on the reaction temperature, although the difference is small. The oxidation rate is almost independent on the reaction temperature.

Almost no deactivation of the reactivity as a function of cycle was seen at any temperature. Figure A3 shows the mass change of the sample during oxidation and reduction as a function of temperature for the two experiments conducted at 850 and 950°C. As the mass level at full reduction and oxidation is approximately constant as a function of cycle, little or no deactivation has occurred. No deactivation was seen at 1000°C. This should be compared to the results with the impregnated particles of NiO/SiO_2, where major deactivation was seen in the reactivity at 950°C. Thus, it seems as if the deactivation is a property of the preparation method. Further, as all of the NiO in the sample seems to be active during the reduction and oxidation cycles, little or no formation of irreversible silicates should occur. The implication of this is that the system NiO/SiO2 may be feasible as an oxygen carrier at higher temperatures.

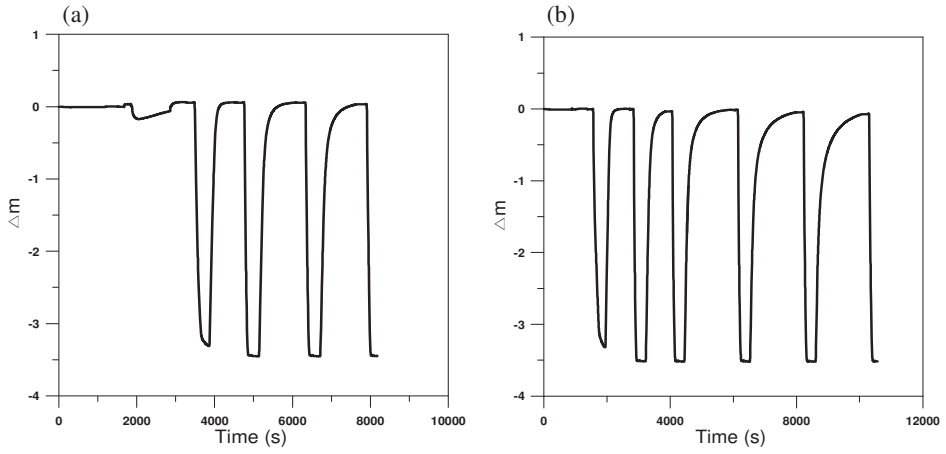

Figure A3: Reactivity as a function of time for the experiments conducted with freeze granulated NiO/SiO_2 at **(a)** 850°C and **(b)** 950°C.